Guan, Li and Yu, Linpo and Chen, George Z. (2016) Capacitive and non-capacitive faradaic charge storage. Electrochimica Acta, 206 . pp. 464-478. ISSN 0013-4686

Access from the University of Nottingham repository:
http://eprints.nottingham.ac.uk/33650/8/2015EA_SI_LG-YLP-GZC-revised%20for%20OpenAccess.pdf

1 **Capacitive and non-capacitive faradaic charge storage**

2 Li Guan [a], Linpo Yu [b], George Z. Chen [a,b,]*

3 [a] *Department of Chemical and Environmental Engineering, Faculty of Engineering,*

4 *University of Nottingham, Nottingham NG7 2RD, UK*

5 [b] *Department of Chemical and Environmental Engineering, and Centre for Sustainable*

6 *Energy Technologies, Faculty of Science and Engineering, University of Nottingham Ningbo*

7 *China, Ningbo 315100, China*

8 *E-mail: george.chen@nottingham.ac.uk

9 **ABSTRACT**

10 This article aims to offer a critical overview of selected literature on capacitive and non-

11 capacitive faradaic charge storage. It is particularly relevant to the concept of

12 pseudocapacitance that is generally described as a result of fast surface **faradaic** processes. In

13 general, faradaic processes represent electron transfer reactions at the interface between an

14 electrode and its contacting solid or liquid electrolyte phase that is able to accept or donate

15 electrons. Obviously, not all faradaic processes can be associated with pseudocapacitance.

16 The question is how to differentiate pseudocapacitance related faradaic charge storage from

17 the others. Therefore, attempts have been made to apply the band model for semiconductors

18 to account qualitatively for the origin of pseudocapacitance. **Capacitive** and **non-capacitive**

19 faradaic processes are then proposed to define and differentiate different charge storage

20 mechanisms in supercapacitor and battery. On the other hand, the unequal electrode

21 capacitance approach and the use of Ca^{2+} in aqueous electrolytes are discussed in relation

22 with enhanced energy capacity of supercapacitors. In addition, the principle of supercapattery

23 as a hybrid device is explained with recent literature examples.

1. Introduction

Since the beginning of human civilisation, the use of energy has been an important means of survival. From burning wood to nuclear energy, the search for and the utilisation of various energy forms form an important part of human history. In recent years, due to the fast depletion of fossil fuel reserves and the increasing negative environmental impact of CO_2 emission, political and economic emphases have been placed on the rapid development of alternative energy technologies, particularly through solar, wind and wave generation. However, the energy derived from these renewable sources must be stored and supplied efficiently in order to be considered a viable competitor to traditional non-renewable options [1]. Energy storage devices including supercapacitor, battery and supercapattery are such devices that are able to store charges in a fast and efficient way and hence help harvest and convert renewable energy to a usable form.

Electrical energy can be electrochemically stored in two fundamental ways: (1) in solid electrode materials relying on fast charge separation and/or chemical reactions of the materials and (2) in liquid electrolytes flowing through a battery of electrochemical cells. The latter is typically represented by redox flow battery. It is unique because energy storage is achieved by reduction and oxidation of redox couples in different electrolytes separated by a membrane and circulated in their own respective spaces [2]. However, due to the requirement for storage and transport of a large volume of the electrolytes, the application for redox flow batteries is limited to stationary needs at present. Great efforts have therefore been made to deeply and comprehensively understand charge storage processes in solid electrode materials in order to develop versatile energy storage devices (e.g. supercapacitors) and improve their performance, which is also of interest of this study.

In general, electrical charge can be stored in the surface and/or solid phases of the electrodes relying on the following storage mechanisms: double layer charging, faradaic

processes, or a combination of both. For instance, the charging-discharging process in an activated carbon electrode is due to charge adsorption or accumulation at the interface between the electrode and the electrolyte, giving rise to the electric double layer (EDL) capacitance. This process is largely electrostatic and non-faradic in nature. It means that ideally, no electron transfer takes place across the electrode/electrolyte interface and the storage of electric charge and energy involves no chemical and physical changes inside the solid phase of the electrode [3]. For the charge storage in a faradaic process, it is generally accepted that large pseudocapacitance arises from electrosorption of ions accompanied by surface redox reactions in which electrons transfer occurs crossing the interface of the current collector and active material.

It is however necessary to point out both EDL and pseudocapactive storage processes are capacitive in nature. In experimental terms, they both offer rectangular cyclic voltammograms (CVs) and linear (or triangular) galvanostatic charge and discharge plots (GCDs) [4]. On the other hand, when the redox active material on electrodes undergoes a reversible or quasi-reversible electron transfer reaction at well separated or isolated sites, current peaks forms on the CV and non-linear potential (or voltage) variation occurs on the respective GCDs. Such electrochemical features are the same or comparable to those of recharge batteries, and should not be used for a capacitance measurement. Thus this type of charge storage is recognised as a non-capacitive faradaic process here.

Consequently, one should not associate all these well-known faradaic processes with pseudocapacitance. The question is how to differentiate pseudocapacitance related faradaic charge storage from the others, namely, the non-faradaic charge accumulation in the EDL and the non-capacitive battery-like behaviours of some electrode materials. Herein, the authors propose to define and differentiate the aforementioned charge storage mechanisms according to **Fig.** 1. Attempts have also been made to account for the origin of pseudocapacitance using

the band model for semiconductors. Further, the recent developments in gaining improved

supercapacitor performance are introduced and discussed in terms of modifications of

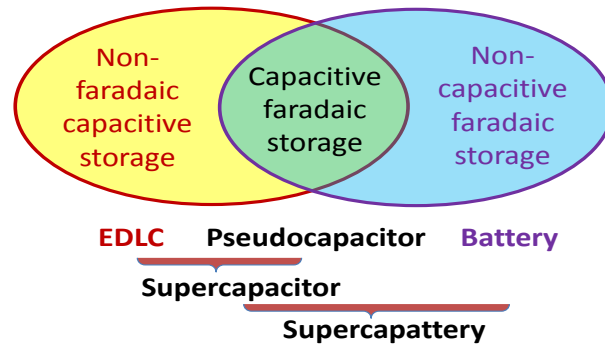aqueous electrolytes and an unequal electrode capacitance approach in laboratory.

Fig. 1. Schematic correlation between EDL capacitor, pseudocapacitor, battery and

supercapattery (= hybrid of supercapacitor and battery) in terms of capacitive and faradaic

charge storage processes.

In order to understand how supercapacitors store large amount of energy and discharge it

for high power applications, it may be easier to start with a review on the fundamentals of the

conventional capacitors that are widely used in electronic devices. In principle, the amount of

charge (Q) stored is in proportion to the voltage (U) applied across the capacitor. The

proportionality is called capacitance (C) which links Q and U according to Eq. (1):

$$Q = CU \tag{1}$$

C is a constant determined by the dielectric constant of the dielectric medium and

proportional to the ratio of the area of the electrode/dielectric interface and the separation

distance between the two electrode plates of the capacitor. When the applied voltage varies

linearly with time (t), i.e. $U = U^o + vt$, where U^o is the starting cell voltage which may be zero

and v is the linear variation rate of voltage, Eq. (1) can be mathematically converted into Eq.

(2), which can be further simplified to Eq. (3) by correlating the current, I, with v [4].

$$\frac{dQ}{dt}=C\cdot\frac{dU}{dt}+U\cdot\frac{dC}{dt}=C\cdot\frac{dU}{dt} \qquad (2)$$

$$C=\frac{dQ}{dt}\Big/\frac{dU}{dt}=\frac{I}{v} \qquad (3)$$

Therefore, the current flowing through a capacitor is in a linear relationship with v, but independent of U. For a constant C, Eq. (3) gives the rectangular I – U plots as shown in **Fig.** 2a, which is also called cyclic voltammograms or CVs. In **Fig.** 2a, the current, I, not only increases proportionally with the increase of v, but also follows the direction of voltage variation, i.e. v is positive when voltage increases and it is negative when voltage decreases. The CV is very useful for evaluation of capacitive behaviour of a device or electrode made from a synthetic pure or composite material.

In practice, galvanostatic charging-discharging (GCD) is also used to calculate the capacitance of a device or electrode material. Under a constant current, according to Eq. (3), the charging process of the capacitor reflects a constant rate of voltage increase and vice versa, the discharging relates to a voltage decrease in a constant rate. As a result, a triangular curve is observed as shown in **Fig.** 2b where the voltage of the capacitor is plotted against the
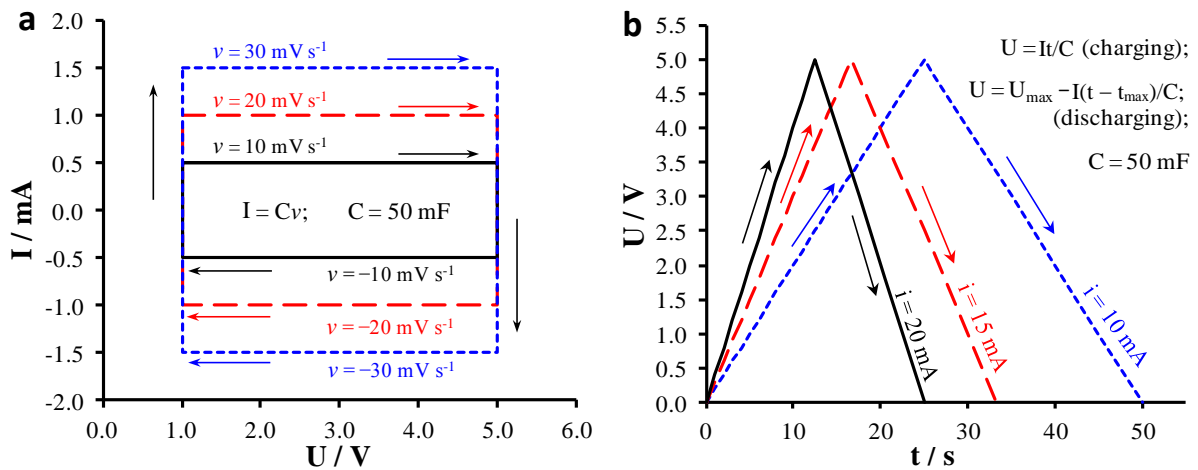
Fig. 2. (a) CVs at indicated linear variation rates of voltage and (b) GCD plots at indicated constant currents as derived from Eq. (3)for a 50 mF capacitor with U_{max} = 5 V. In the GCD plots in (b), $t_{max} = U_{max}C/I$ [4].

1   time during a cycle of constant current charging and discharging.

2   When the capacitor is charged, a voltage, U, will build up across the two electrodes. The

3   amount of energy (ε) stored and the power output (P) from the capacitor can be determined

4   through a series of calculations below. At first, the work, $d\varepsilon$, done in a short time to move a

5   small quantity of charge, dQ, to be accumulated at the electrode/dielectric medium interface

6   can be calculated from Eq. (4) by considering $d\varepsilon = \mathrm{U}d\mathrm{Q}$. If the heat loss during charging is

7   insignificant, the total energy stored in the capacitor is then determined after integration. It is

8   worth noting that a practical capacitor has always a maximum tolerable voltage, U_{max}, beyond

9   which the dielectric or ionic medium will break down (or decompose). Thus there is a

10   maximum energy capacity, ε_{max}, that can be correlated to U_{max} and the capacitance, C, which

11   is the property of the capacitor (or electrode) material used.

12
$$d\varepsilon = \mathrm{U} \cdot d\mathrm{Q} = \frac{\mathrm{Q}}{\mathrm{C}} \cdot d\mathrm{Q} \tag{4}$$

13
$$\varepsilon_{max} = \int_0^Q \frac{\mathrm{Q}}{\mathrm{C}} d\mathrm{Q} = \frac{1}{2} \cdot \frac{\mathrm{Q}^2}{\mathrm{C}} = \frac{\mathrm{Q} \cdot \mathrm{U}_{max}}{2} = \frac{\mathrm{C} \cdot \mathrm{U}_{max}^2}{2} \tag{5}$$

14   Secondly, it is to determine the power output, P, using the time needed to fully discharge

15   the capacitor as expressed in Eq. (6):

16
$$\mathrm{P} = \frac{\varepsilon}{\mathrm{t}} = \frac{\mathrm{C} \cdot \mathrm{U}^2}{2 \cdot \mathrm{t}} \tag{6}$$

17   In fact, Eq. (6) can be further developed into Eq. (7) by taking the equivalent series

18   resistance (ESR) and the working load (R_L) into account since the ESR is the unavoidable

19   nature of an electric power source. The power transferred from the source to the load can also

20   be derived from $\mathrm{P} = i\mathrm{U} = i^2 \mathrm{R}_L$.

21
$$\mathrm{P}_{max} = \left(\frac{\mathrm{U}_{max}}{\mathrm{R}_L + \mathrm{ESR}} \right)^2 \mathrm{R}_L = \frac{\mathrm{R}_L \cdot \mathrm{U}_{max}^2}{(\mathrm{R}_L + \mathrm{ESR})^2} \tag{7}$$

22   where $\mathrm{U} = \mathrm{I} \cdot (\mathrm{R}_L + \mathrm{ESR})$ with the current passing through the circuit shown in **Fig.** 3. It is

obvious that the maximum power, P_{max}, can be reached at $R_L = ESR$, leading to Eq. (8) which shows P_{max} is a function of U and ESR, but independent of C, although C determines the amount of energy stored in the capacitor. Furthermore, by bringing Eq. (8) into Eq. (6), the shortest discharging time, t_{min}, can be obtained, which is practically useful and important for device design, such as supercapacitor supported systems. However, Eq. (9) has currently not gained enough recognition or attention in terms of reporting data and analyses. This is somehow unfortunate because highlighting the maximum power of supercapacitors against that of batteries without mentioning the lasting time the device can work at the high power may confuse or even mislead readers and customers who are not well informed.

$$P_{max} = \frac{ESR \cdot U^2}{(ESR + ESR)^2} = \frac{U^2}{4 \cdot ESR} \tag{8}$$

$$t_{min} = \frac{C \cdot U^2}{2 \cdot P_{max}} = \frac{C \cdot U^2}{2 U^2/(4 \cdot ESR)} = 2 \cdot C \cdot ESR \tag{9}$$
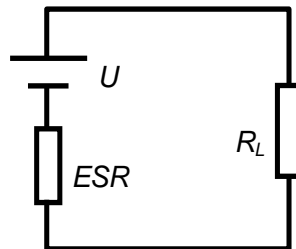
Fig. 3. The electric circuit for derivation of P_{max} and t_{min} (cf. Eq. (7) - (9)). R_L is the resistance of the working load, U and ESR are the voltage and the equivalent series resistance of the power source, respectively.

2. Non-faradaic capacitive storage

The capacitance of a conventional capacitor typically ranges between $10^{-6} - 10^{-2}$ F, therefore the energy stored in the capacitor is too small for meaningful practical uses. For

example, for a 50 mF capacitor with an applied voltage of 100 V, the energy stored is only

250 J. Hence, in recent years, supercapacitors, also known scientifically as electrochemical

capacitors, become an important development in the field of energy storage and conversion.

The capacitance of commercial supercapacitors can commonly reach to 10^2 - 10^4 F. However,

this huge difference in capacitance does not change the fact that a supercapacitor is still a

capacitor. There is no doubt that the behaviour of a supercapacitor should also be governed

by all the equations discussed in the previous section and be the same as those in **Fig.** 2,

showing the rectangular CVs and triangular GCD plots.

2.1. Supercapacitors with double layer capacitance

EDL capacitors are the first generation supercapacitors in which charge storage occurs in

the electric double layer at the electrode/electrolyte interface and relies mainly on charge

separation. Although this storage mechanism is the same as that in the traditional electrolytic

capacitors, the specific capacitance (C_s, F g^{-1}) increases drastically by taking advantages of

the high porosity and large specific surface area (m^2 g^{-1}) of the active electrode materials, e.g.

activated carbon. **Fig.** 4 illustrates the displaced ions in the electrolyte in the interconnected

pores of the electrode and the balancing charges (i.e. excess of electrons or holes) on the wall

surfaces of the pores that are formed between the packed activated carbon particles.

Assuming that the electrode/electrolyte interface has true capacitance of $0.1 - 0.3$ F m^{-2} and

the specific surface area of activated carbons is 1000 m^2 g^{-1}, the specific capacitance, C_s, of

activated carbon can be calculated to range from 100 to 300 F g^{-1}. However, in many cases,

the specific capacitance of activated carbons is usually about 100 F g^{-1} [5]. The cause is

largely because the high porosity and specific surface area make activated carbons weaker

and less conducting. The other issue is that not all the internal surface area, such as those of

the wall of micro-pores, can be accessed by ions in the activated carbon for charge storage.
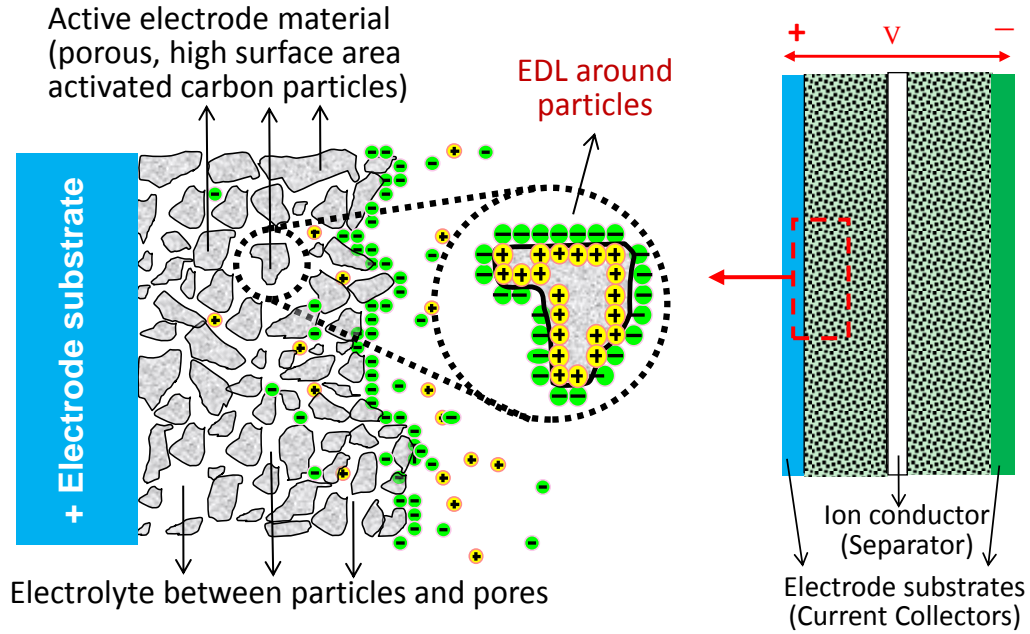
Fig. 4. Schematic illustration of charge storage mechanism in an EDL capacitor using porous and high surface area activated carbon particles as the electrode.

Therefore, nanomaterials, such as carbon nanotubes (CNTs) and graphenes, have been suggested as a good solution to solve the problems [6-8]. In addition to the extra high specific surface area and the construction of three dimensional structures, CNTs and graphene can also benefit the electron conduction through carbon structures and the ion conduction through the liquid electrolyte contained in the carbon structures [9].

In particular, CNTs have been widely studied and recognised as suitable materials for applications in supercapacitors with the acknowledgement of the novel structure, narrow pore size distribution, low resistivity and high mechanical strengths [10-13]. Comparing with the porous activated carbon in the upper bound, CNTs have exhibited higher capacitance, e.g. 102 F g^{-1} for multi-walled CNTs [14], and 180 F g^{-1} for single-walled CNTs [15]. It has also been reported that a single-walled CNT based supercapacitor showed a promising power capability of 20 kW kg^{-1} with a maximum energy capacity of around 7 Wh kg^{-1} at 0.9 V in a solution of 7.5 N KOH [15]. On the other hand, factors that affect the performance of CNT

based supercapacitors have been extensively researched from the aspects of structural

properties (e.g. diameter, length and pore size), graphitisation by heating and modification via

chemical activation, functionalization and surface treatment [6]. Among these, it was found

that boiling CNTs in a mixture of concentrated acids was one of the most effective methods

to modify CNT surfaces and introduce functional groups which play an important role on the

capacitance improvement [16, 17]. However, effects of the electrolytes on the capacitance of

supercapacitors have attracted relatively less attention [18-20]. It is acknowledged that

cations, anions and pH of the electrolyte may all affect the performance of a particular

electrode material. In this paper, CNTs and activated carbon electrodes are investigated in

correlation with the concentration and nature of ions, temperature, and the CNT surface

functional groups. The results are particularly interesting, confirming different affinities of

cations in the electrolyte (i.e. Ca^{2+} and K^+) towards the oxy-groups on CNT surfaces and

workability of this type of supercapacitors at temperatures below $-60\ ^\circ C$.

2.2. Effects of electrolyte

In the experiment, the effect of the electrolyte concentration on the electrochemical

behaviour was investigated by performing cyclic voltammetry in various KCl aqueous

solutions using a 5 mm dia. graphite disc electrode coated with a thin layer of activated

carbon (Haycarb, loading: 0.2 mg or 1.0 mg cm^{-2}) as the working electrode. A graphite rod

was used as the counter electrode and the Ag/AgCl couple used as the reference electrode.

The resulting CVs are shown in **Fig.** 5. These results agreed to certain extend with some

reported observations in literature that EDL capacitance increased with the increase of the

electrolyte concentration [21, 22], i.e. the CV current kept increasing until the concentration

of the KCl solution reached to 1.0 M (see **Fig.** 5a). Interestingly, the CVs observed with

further increasing the concentration to 3.0 M had shown insignificant changes in current as
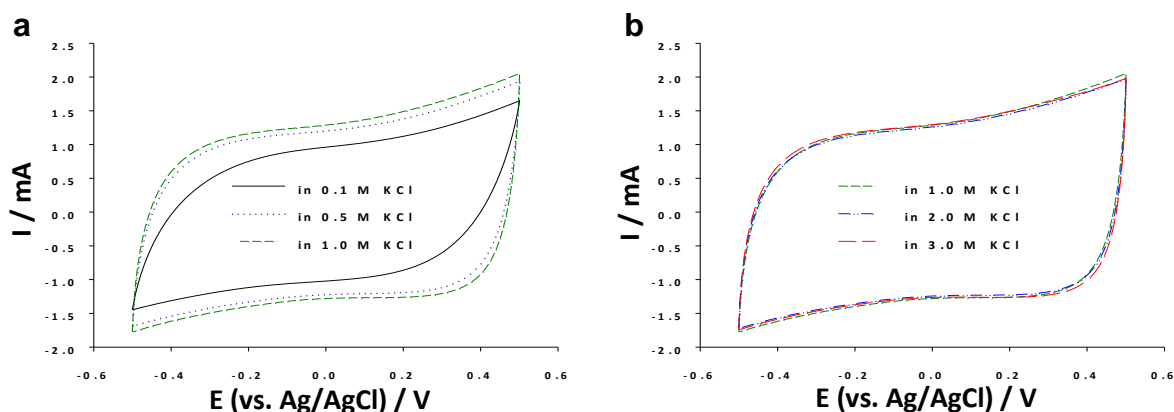
Fig. 5. (a,b) CVs of the Haycarb carbon electrode (loading: 1 mg cm^{-2}) in KCl aqueous solutions with different concentrations as indicated. Potential scan rate: 100 mV s^{-1}.

shown in **Fig.** 5b. It was likely that the active sites on the surface of Haycarb carbons were saturated by the ions in the electrolyte while recording the previous CVs and became inaccessible even though the ion concentration was significantly increased.

The capacitance improvement from the surface modification with functional groups is well demonstrated by the significant current increase in the CVs recorded in 1.0 M KCl using a 6.5 mm dia. graphite disc electrode coated with acid-treated CNTs (**Fig.** 6b), in comparison with those of as-received CNTs (**Fig.** 6a). It is acknowledged that using concentrated acids (a mixture of H_2SO_4 and HNO_3 with 3:1 v:v in current case) to treat raw CNTs can introduce oxygen-containing groups to the CNT surfaces, such as carbonyl, carboxyl and hydroxyl groups or simply oxy-groups [23]. These functional groups not only improve the hydrophilicity of the CNTs, but also enhance the overall charge storage performance [24]. The pair of broad peaks on the CV of **Fig.** 6b indicates the oxy-groups on the surfaces of the acid-treated CNTs had undergone a reversible redox or faradaic reaction. Since the CV with the broad peaks still remains fairly rectangular, it can still be regarded as being capacitive. Thus, the acid-treated CNTs exhibited a much higher specific capacitance of 60 F g^{-1} than that of the as-received CNTs (9.1 F g^{-1}), because the charge storage process of the former
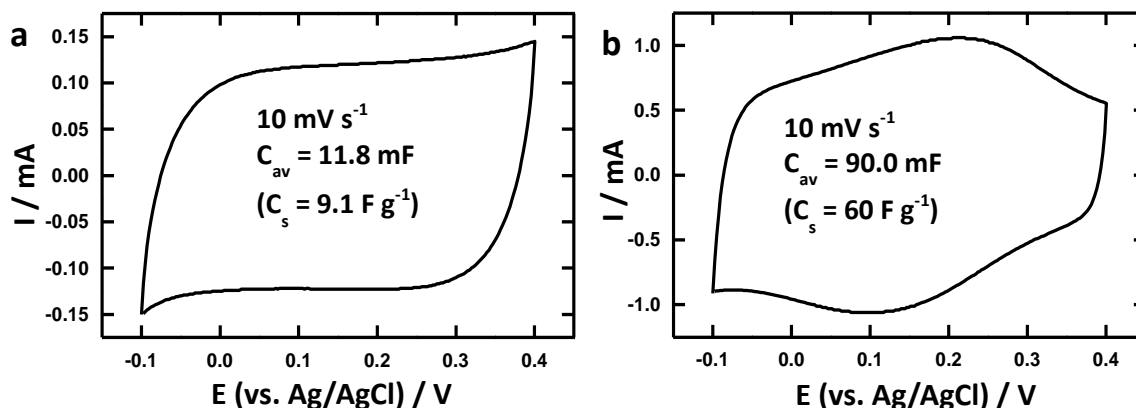
Fig. 6. CVs of (a) as-received CNT (1.3 mg) and (b) acid-treated CNT (1.5 mg) in 1.0 M KCl aqueous solution with indicated electrode capacitance averaged over the potential range (C_{av}) and specific capacitance (C_s). Potential scan rate: 10 mV s^{-1}.

involved both EDL capacitance and pseudocapacitance. It is worth mentioning that **Fig.** 6b shows that the increased charge storage occurs mostly in the middle of the potential window. This means that in a symmetrical capacitor, the increased charge capacity would be utilised at low voltages and hence contribute little to the energy capacity. It would be more meaningful to use such acid-treated CNTs or activated carbon in an asymmetrical supercapacitor so that the charge storage can increase at higher cell voltages to give rise to larger energy capacity. In such cases, the increased charge storage capacity can be further exploited together with the unequal electrode capacitance strategy as will be discussed in the later section.

The influence of cations in the electrolyte on capacitance was also investigated by recording CVs in CaCl$_2$ and KCl solutions, respectively. It was particular interesting to observe that the CVs of acid-treated CNTs recorded in the CaCl$_2$ solutions generally exhibit greater currents than those in the KCl solutions (see **Fig.** 7a and b). These differences could be attributed to the greater affinity of the Ca^{2+} ions than K$^+$ towards the oxy-groups on the CNT surfaces [25]. In fact, it has been mentioned in some early studies [26, 27] that the so called Calcium Ionophore A23187 or Antibiotic A23187 has high selectivity for binding and
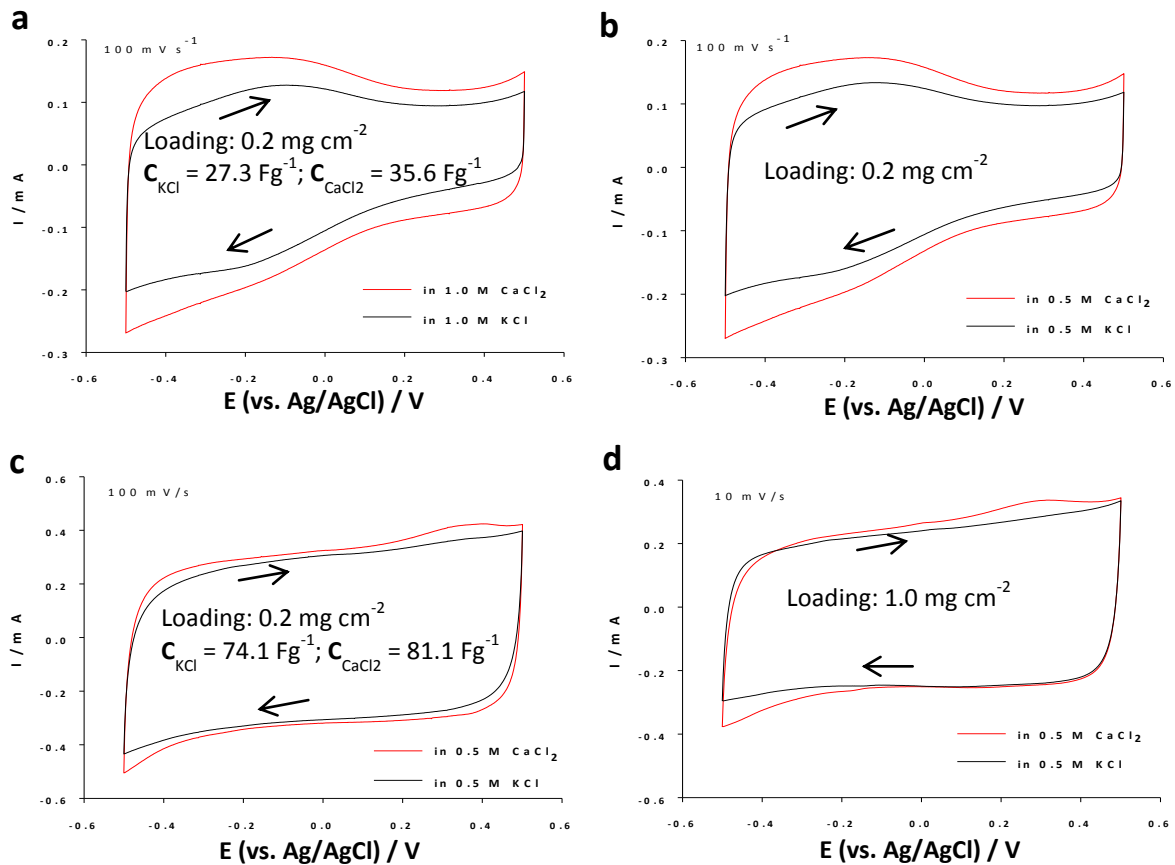
Fig. 7. CVs of (a,b) acid-treated CNT recorded in (a) 1.0 and (b) 0.5 M solutions of CaCl$_2$ (red curves) and KCl (black curves) [25], and of (c,d) Haycarb carbon both recorded in 0.5 M solutions of CaCl$_2$ (red curves) and KCl (black curves). Note that the electrode loading and scan rate are different and respectively indicated along with some of the capacitance values. Arrows indicate the direction of the potential scan. The CNTs were treated using the same method as those in **Fig.** 6, but in a recent batch [25].

transporting the Ca^{2+} ion over other cations, such as Na$^+$, K$^+$ and Mg^{2+} ions in biological systems. Therefore, if we could interpret this high Ca^{2+} ion selectivity of A23187 as the various oxygen containing groups in the ionophore molecule formed a Ca^{2+} ion binding site/cavity as illustrated in **Fig.** 8a, the unique interaction between Ca^{2+} and the CNT surface oxy-groups can be similarly explained in the current case. As schematically illustrated in **Fig.** 8b, it can be assumed that the oxy-groups on CNT surfaces have high selectivity or affinity

for Ca^{2+} ions. This assumption is in agreement with many previous studies involving interactions between CNTs and Ca^{2+} ions [26-29]. It was also reported that according to molecular dynamic simulation, the interaction between the carboxylate group on CNTs and Ca^{2+} ions are more favourable over K^+ and Na^+ ions [28]. As a result of the greater affinity of the surface oxy-groups with Ca^{2+} than with K^+, about 30% capacitance increase was observed as derived from the CVs (red curves) in **Fig.** 7a and b. Moreover, in an experimental study, as-prepared CNTs (which must contain surface oxy-groups) were demonstrated to be effective scaffold materials for osteoblast proliferation and bone formation, thanks to partly the ability of the CNTs to conduct Ca^{2+} currents [29]. This means the structural arrangement of the oxy-groups on the CNT surfaces are suitable for binding Ca^{2+} via Reaction (1) below.

$$2\,R\text{-}COOH + Ca^{2+} + 2\,e \leftrightarrow (R\text{-}COO^-)_2Ca^{2+} + 2\,H_{(ad)} \tag{1}$$
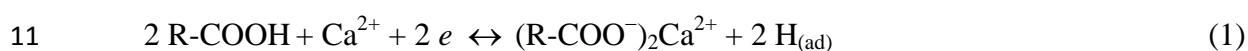
In addition, the fact that each Ca^{2+} ion has two positive charges could be another important cause for the increase of the specific capacitance. To compare a 1:1 type electrolyte with a 1:2 type, e.g. KCl vs. $CaCl_2$, a simple way was adopted in this work to halve the concentration of the latter, i.e. 1.0 M KCl vs. 0.5 M $CaCl_2$. It is obvious that the CV current observed in 0.5 M $CaCl_2$ (red curve in **Fig.** 7b) was greater than that observed in 1.0 M KCl (black curve in **Fig.** 7a), leading to a higher specific capacitance. It is noticeable that the CNT electrode was much more sensitive to replace KCl with $CaCl_2$ than to the doubled electrolyte concentration as the concentration change (from 1.0 to 0.5 M) had a fairly small influence on the CV current and shape. This is indicative of the charge (or ion) storage in the electrode being determined mainly by the available sites on the CNT surface for ion sorption, instead of the number of ions in the electrolyte [25].

However, when similar investigations were carried out using a Haycarb carbon electrode, the greater current previously observed in $CaCl_2$ solutions became insignificant (see the unpublished results shown in **Fig.** 7c and d). This is because there was much less oxy-groups

1 in the Haycarb carbons and the binding cavity formed between the carbon particles may not

2 be compatible with the Ca^{2+} ion in terms of size and shape.
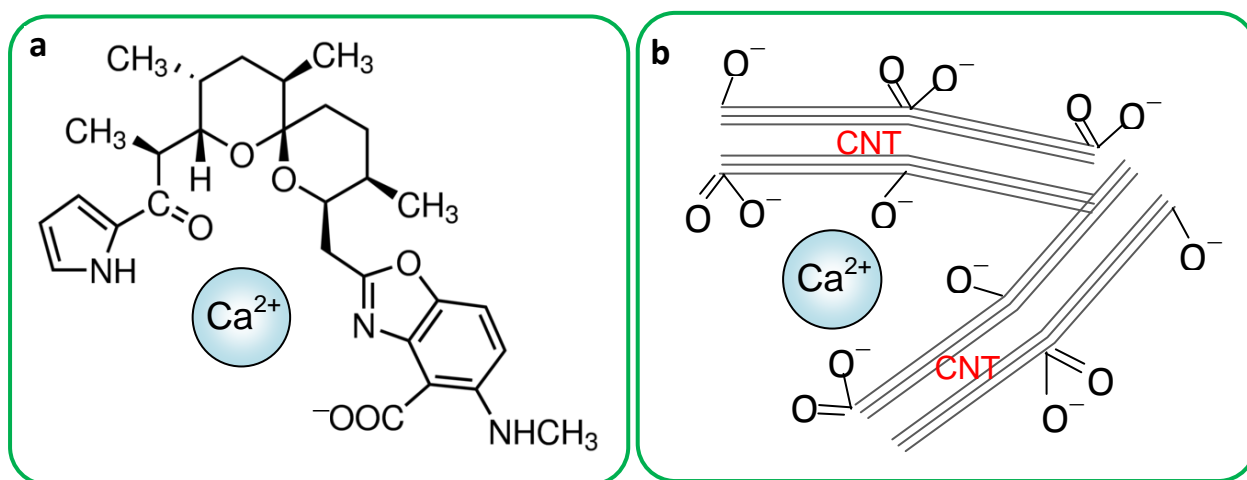
5 **Fig. 8**. Schematic illustration of the binding of a Ca^{2+} ion by the oxy-groups in the cavity

6 formed (a) in the Calcium Ionophore A23187 molecule, and (b) in between the acid-treated

7 CNTs [25].

9 On the other hand, for sub-zero temperature applications, organic electrolytes are

10 commonly used [30-32], but they have lower conductivity and are more expensive than

11 aqueous electrolytes. Mixing water with an additive may lead to low temperature benefits.

12 The binary phase diagram of water and formamide (FA) is shown in **Fig.** 9a with a eutectic

13 temperature of −46 ^{o}C [25]. The binary phase diagrams of water and some simple salts are

14 presented **Fig.** 9b, showing eutectic temperature below −50 ^{o}C on the $CaCl_2$-H_2O curve. Thus,

15 by dissolving $CaCl_2$ into the FA-H_2O mixture, a novel organoaqueous electrolyte was

16 prepared and proven to be able to work at temperatures below −60 ^{o}C [25].

17 **Fig.** 10a and 10b compare the CVs of the CNT electrode measured in different

18 electrolytes at 20 $^{\circ}$C and −60 $^{\circ}$C, respectively. It can be seen that the solution of $CaCl_2$ in FA

19 is not a good electrolyte, but addition of FA into water does not affect very much the

20 electrochemical behaviour. Particularly, **Fig.** 10b confirms the $CaCl_2$-FA-H_2O mixture to be

1
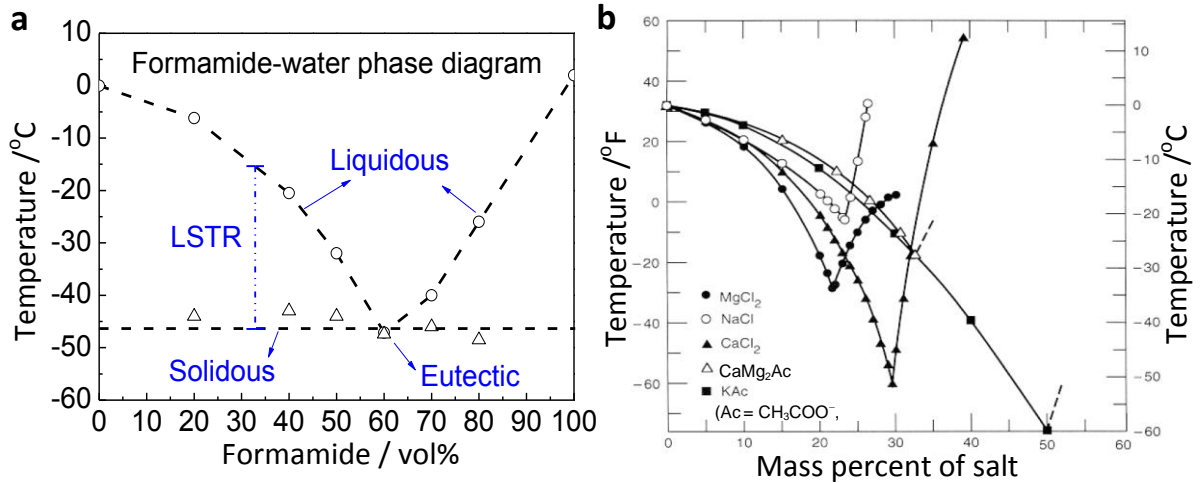
Fig. 9. (a) The formamide-water phase diagram. The dashed lines are presented as a vision

guide [25]. (b) Phase diagrams of $CaCl_2$, $MgCl_2$, NaCl, $CaMg_2Ac_6$ (CMA), and KAc, Ac=

CH_2COO^- [33].

5
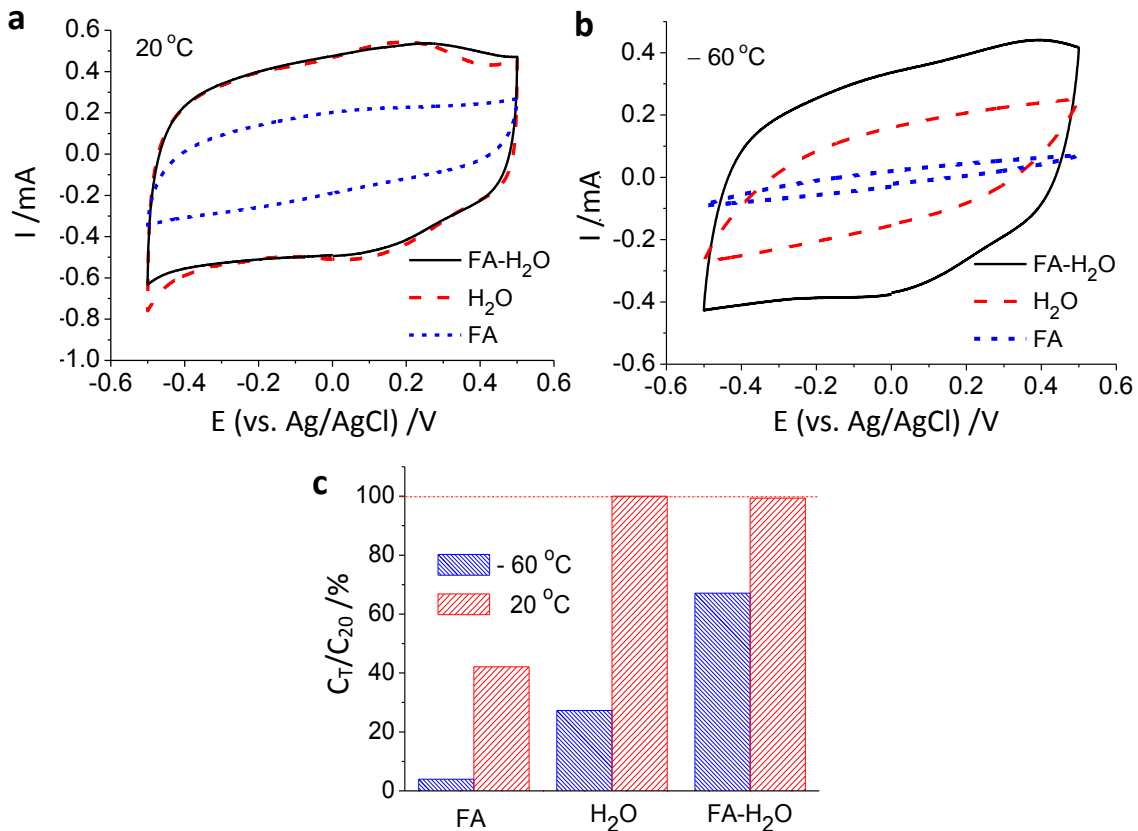
Fig. 10. (a,b) CVs and (c) C_T/C_{20} (= 100×capacitance at designated temperature / capacitance

at 20 °C) of CNT electrode at (a) 20 °C and (b) −60 °C in the $CaCl_2$ solution of FA (1.0 M),

H_2O (2.0 M) and mixed FA-H_2O (1:1, v:v, 2.0 M). Potential scan rate: 100 mV s^{-1} [25].

1   very good for low temperature uses. **Fig.** 10c presents the capacitance retention of the CNT

2   electrode as derived from the rectangular CVs in **Fig.** 10a and 10b. At 20 $^{\circ}$C, the measured

3   specific capacitance, C_s, was almost the same in $CaCl_2$-H_2O (108.3 F g^{-1}) and $CaCl_2$-FA-H_2O

4   (107.6 F g^{-1}), whereas at -60 $^{\circ}$C, C_s in $CaCl_2$-FA-H_2O was still 72.7 F g^{-1} (67% capacitance

5   retention), which is more than double of the value measured in $CaCl_2$-H_2O. Hence, it can be

6   concluded that the $CaCl_2$-FA-H_2O mixture is an excellent electrolyte for capacitive charge

7   storage in partially oxidised CNTs at sub-zero-temperatures.

8

9   **3. Capacitive faradaic charge storage**

10   Charge storage in pseudocapacitive materials involves electron transfer reactions and

11   hence the reduction or oxidation changes in the electrode materials, which are also referred to

12   as faradaic reactions or processes. However, not all faradaic processes can contribute to

13   pseudocapacitive behaviours. Despite the electron transfer reactions in a rechargeable battery

14   or a fuel cell are also faradaic in nature, the respective current-voltage relations in these

15   electrochemical devices differ significantly from that in a capacitor [9]. Such energy storage

16   and discharge can be regarded as non-capacitive faradaic processes. The performance

17   difference between capacitive and non-capacitive faradaic processes could be the effect of

18   localised and delocalised valence electrons [4, 34].

19

20   3.1. Reversible non-capacitive faradaic process in electrode coatings

21   Non-capacitive faradaic process can result from localised reversible electron transfer

22   reactions in a redox active coating on an electrode. When this happens, the CV should be a

23   bell-shaped curve as displayed in **Fig.** 11a [3, 34]. The potential of the current peaks on the

24   CV is determined by the redox potential of the material. The current response towards the

25   potential change can be expressed as Eq. (10), which is derived from the Nernst and Randles-

1   Sevcik equations [35].

2
$$i = \frac{n^2 F^2 A \Gamma_t v \exp\left[\left(E - E^o\right)\dfrac{nF}{RT}\right]}{RT\left\{1 + \exp\left[\left(E - E^o\right)\dfrac{nF}{RT}\right]\right\}}$$
(10)

3   where n is the number of electrons transferred between the reduced and oxidised sites, F the

4   Faraday constant, A the area of electrode, Γ_t ($=\Gamma_o + \Gamma_r$) the total surface covered by the

5   reduced and oxidised sites and v is the potential scan rate, R the ideal gas constant and T the

6   absolute temperature. Due to the strong dependence of the electrode reaction on potential, the

7   GCD plots in **Fig.** 11b show potential plateaux over a narrow potential range. Nevertheless,

8   the faradaic reaction took place in the electrode materials is reversible as the shapes of the

9   CVs and GCDs are symmetrical in horizontal and vertical orientations, respectively [4].

10   The cause for CVs or GCD plots in **Fig.** 11 are not rectangular or triangular like those

11   shown in **Fig.**2 may be explained from a view point of electron energy states. As electron

12   energy states are separated in isolated molecules or insulators, the energy levels of the filled

13   and vacant states are singular and the process that electron inject to (or remove from) an

14
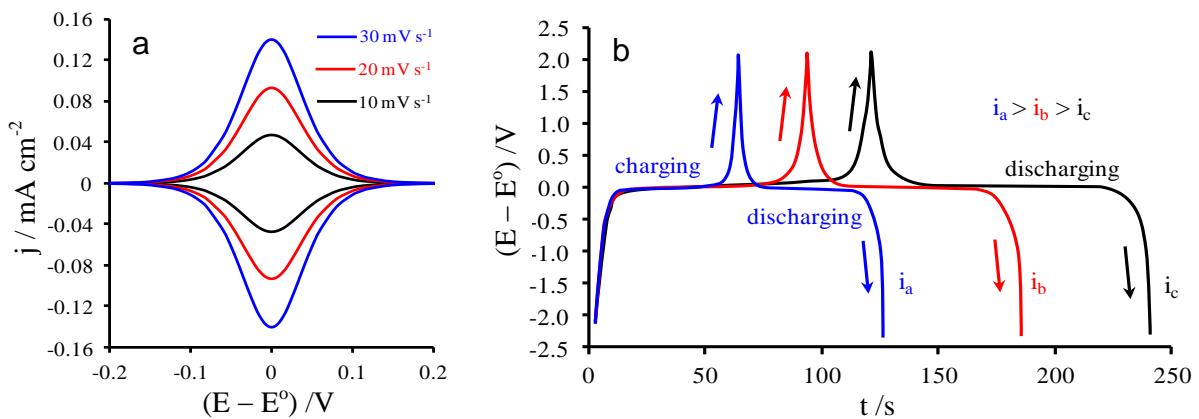
15

16   **Fig. 11.** (a) CVs at indicated potential scan rates and (b) GCD plots at indicated constant

17   currents of $i_a > i_b > i_c$ for a reversible faradaic reaction with localised electron transfer to and

18   from isolated redox sites on the electrode [4].

1   electrode may take place in very well separated redox active sites. In other words, because

2   these redox centres are non-interactive or electronically isolated from each other but have

3   equal or fairly close energy states, electron acceptance or donation occurs at potentials very

4   close to each other, resulting in the peak shaped CV in a narrow potential range as shown in

5   **Fig.** 11a. However, if these redox active sites can interact with each other due to either short

6   separations or good electronic conductivity or both, their energy states can merge into a broad

7   band with negligibly small differences between the neighbouring states. Such a situation

8   corresponds to the conduction band in semiconductors, including most transition metal oxides,

9   and is also comparable with the electron delocalisation in conjugated chemical bonds, as in

10 electronically conducting polymers (ECPs), resulting from overlapping electron orbits

11 between neighbouring atoms. As a result, electron transfer into (or from) each energy state in

12 this broad band becomes continuous over a wide range of potentials, which is responsible for

13 the constant current flow and hence the rectangular CV.

14

15 3.2. Pseudocapacitance from delocalised electrons

16   The above analysis is derived from the band theory for semiconductor [35], which can

17 also be applied for qualitative description of the capacitive faradaic process for charge

18 storage in pseudocapacitive materials. **Fig.** 12a illustrates the distribution energy states in

19 three different materials, namely, metals, semiconductors, and insulators. Electron energy

20 states of metals are completely overlapped, enabling free electron mobility in response to an

21 electrical field. Unfortunately, no capacitance can be achieved since charges cannot be stored

22 in a geometric location. Within an insulator, redox active sites are unable to interact with each

23 other electrically and hence behave like individual molecules. This means localised electron

24 transfer from the electrode substrate to each of the redox active sites in a narrow potential

25 range and hence a current peak on the CV. Such processes are shown in **Fig.** 12b on the CV

1 of an electro-deposited ferrocenyl polymer coating on a Pt disc electrode in an organic

2 electrolyte [36]. The large peak couple, a2/c2, results from the ferrocenyl groups, and the

3 smaller couple, a3/c3, from the polymer. As previously mentioned, a narrow peak would

4 form on the CV if the non-capacitive faradaic electrode reaction takes place in which electron

5 transfer reaction occurs at separated sites (e.g. the ferrocenyl groups) with energy states very

6 comparable to each other.

7 As shown in **Fig.** 12a, semiconductors are featured by their slightly separated filled

8 valence band and the vacant conduction band. When the applied potential is suitable for

9 electron excitation, electrons in the valence band can jump over to the conduction band and

10 become delocalised. At the same time, mobile holes are left in the valence band. Thus,

11 although the energy gap between the broad valence and conduction bands is small, the

12 continuous electron dislocation and hole production over the relatively wider potential range

13 give rise to the constant capacitive current flow as shown in **Fig.** 12c. These CVs were

14 recorded in 0.5 M LiCl using an electrode coated with thin films of MnO_2 with different

15 thicknesses.[37] Due to electron dislocation in semiconductor MnO_2 coatings conducted

16 amongst redox sites which interacted actively and continuously with each other between

17 neighbouring states, rectangular CVs were observed. This type of charge storage process is

18 the so called capacitive faradaic process.

19 It is noteworthy that mixed forms of the above two types of charge storage mechanisms

20 are also observed in many cases with the development of advanced nanomaterials for

21 supercapacitor applications. For instance, it has been reported that the electro-deposited

22 polyaniline (PAN) nanofibrils were able to store charges relying on both pseudocapacitance

23 and EDL capacitance, giving rise to a maximum specific capacitance for PAN.[38] It was

24 also suggested that both charging processes were carried out in parallel. In other words, non-

25 faradaic capacitive, capacitive faradaic and non-capacitive faradaic reactions have all

1   proceeded in PAN and made contributions to the overall charge storage.
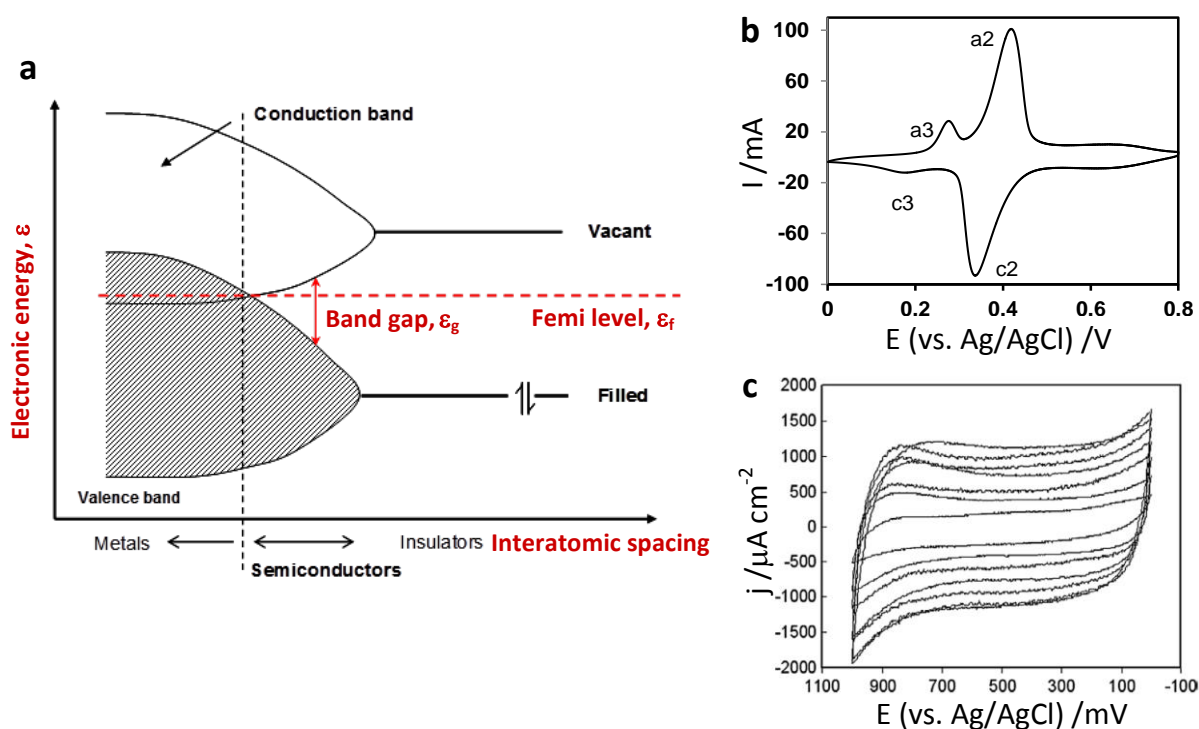
2

3   **Fig. 12.** (a) Schematic illustration of the band theory [34]. (b,c) CVs of (b) an

4   electrodeposited ferrocenyl bithiophenic polymer coating on Pt disc electrode in an

5   acetonitrile electrolyte at 20 mV s^{-1} [36] and (c) MnO$_2$ thin films of increasing thickness

6   formed by redox deposition on graphite electrode in 0.5 M LiCl at 25 mV s^{-1} [37].

7

8   In the work, the PAN nanofibrils were potentiostatically deposited at 1.0 V vs. Ag/AgCl

9   on a platinum disc electrode (1.6 mm in diameter) from a solution containing 0.25 M aniline

10   monomer and 1.0 M HCl. The polymerised PAN can be presented by the chemical formula in

11   **Fig.** 13a, showing the faradaic charge storage stoichiometry of PAN. The α number is used to

12   express the fraction of the charge of an electron that each aniline monomer unit shares, e.g.

13   0.5 electron per monomer (α = 0.5) is needed to oxidise the polymer from its fully reduced

14   state (leucoemeraldine) to the partially oxidised state (emeraldine). Upon oxidation, the

15   polymer is doped by counter anons, A$^-$, to balance the positive charges in the polymer chains
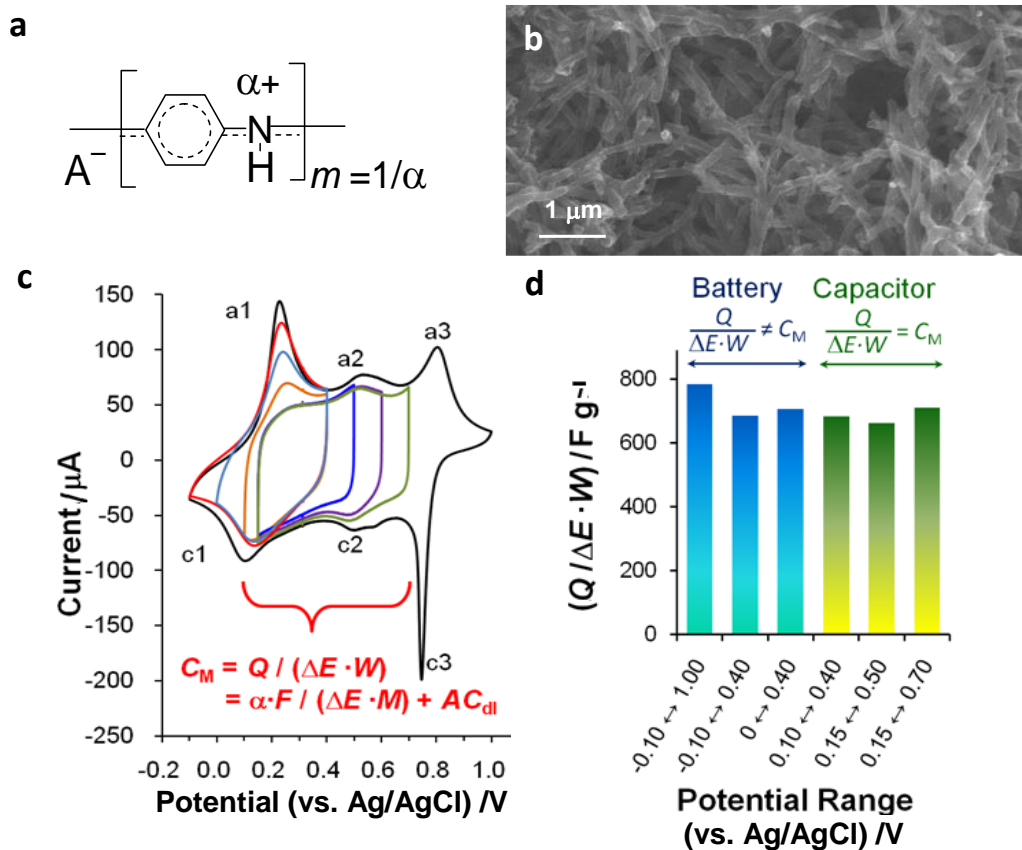
Fig. 13. (a) Faradaic charge storage stoichiometry of PAN, (b) SEM image and (c) CVs of PAN nanofibrils in 1.0 M HCl at 20 mV s^{-1} in different potential ranges [38]. (d) C_s or the $Q/(\Delta E \cdot W)$ ratio derived from the CVs in (c) with indicated potential ranges.

along which the electrons are delocalised amongst several neighbouring monomers. The prepared PAN nanofibrils had a thickness in the range of $50 - 150$ nm and were interconnected to form a porous structure as shown in **Fig.** 13b.

CVs were also recorded in 1.0 M HCl in different potential ranges to characterise capacitive behaviours of the PAN nanofibrils. It can be seen in **Fig.** 13c that the CV shape changes significantly with positively shifting the negative potential scan limit and becomes rectangular with diminishing or disappearance of peak a1. This indicates the PAN behaved like a capacitor within a narrow potential range in which reversible conversion between leucoemeraldine and emeraldine was the major electrode reaction [38]. With further

extension of the potential window, PAN however behaved like a battery since the polymers started experiencing irreversible changes caused by the oxidation to the fully oxidised state, pernigraniline. Again, due to the non-capacitive or battery-like behaviour of PAN, the peak shaped CVs should not be used for the capacitance measurement as the large peak current will lead to a misleading ultra-high capacitance value [39].

In contrast, the specific capacitance of PAN can be calculated as below based on the rectangular CVs in **Fig.** 13c after combining faradaic and double layer contributions,

$$C_s = \frac{Q}{\Delta E \cdot W} = \frac{\alpha \cdot F}{\Delta E \cdot M} + AC_{dl} \qquad (11)$$

where F is the Faraday constant, ΔE the potential range, M the molecular mass of the monomer unit in the polymer, A the specific area (m^2 g^{-1}) and C_{dl} the double layer capacitance per unit true area of the material (F m^{-2}). In accordance with the redox mechanism of PAN, α varies with ΔE, but the relation may not be linear. Thus the maximum value of C_s can appear at smaller values of α and ΔE [38, 40], where the reversible redox reactions (capacitive faradaic reactions) of PAN predominate. In this situation, electron delocalisation occurs along the polymer chains to enable high conductivity and pseudocapacitance. However, it is worth pointing out that the C_s values derived from the rectangular CVs of PAN are generally smaller than those Q/(ΔE.W) ratios measured over the wide potential range in which battery-like behaviour dominated as shown in **Fig.** 13d. This is due to the insulating-to-conducting phase transition in the polymer leading to the large current of peak a1 [41].

Interestingly, measuring capacitance based on a non-capacitive faradaic charge storage process does not come singly but in pairs, giving misleading results. It was reported that combination of an activated carbon electrode with a redox electrolyte containing $CuCl_2$ could increase significantly the charge storage capacity of activated carbon, compared with a

1   conventional inert electrolyte as shown in **Fig.** 14a [42]. As expected, a huge current peak

2   was observed because in the acidic media (1 M HNO_3), $CuCl_2$ reacted with the oxy-groups on

3   the surface of the activated carbon electrode by self-reduction to form an additional redox
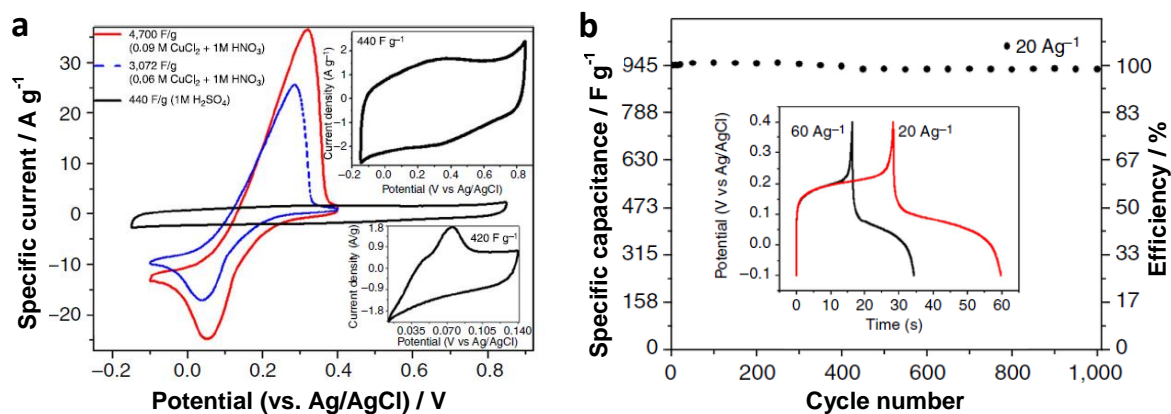
4

5   **Fig. 14.** (a) CVs of activated carbon in an acidic aqueous solution with and without $CuCl_2$ at

6   5 mV s^{-1}. The top inset is the magnification of the CV in a 1 M H_2SO_4 solution and the

7   bottom inset shows the curve in 1 M HNO_3 and 0.12 M $CuSO_4$. (b) The GCD cycling

8   performance of the as-prepared electrode in 1 M HNO_3 and 0.06 M $CuCl_2$ aqueous

9   electrolyte solution at 20 A g^{-1}. The inset shows charge-discharge curves at different current

10 densities.

11

12 layer of CuCl. Unfortunately, the CVs in **Fig.** 14a were misused to derive an ultrahigh but

13 misleading specific capacitance of 4700 F g^{-1}. The related GCD plots (**Fig.** 14b) are akin to

14 those of rechargeable batteries other than the triangular plot of a capacitor as shown in **Fig.**

15 2b. Similar to the aforementioned cases, although this electrode-electrolyte reaction was

16 faradaic in nature, it took place at fixed or localised redox activated sites (C=O bond on the

17 carbon surface) which are not interactive with each other to generate pseudocapacitance.

18   However, in the paper, the performance characteristics were still calculated based on the

19 peak shaped CVs regardless the origin of the charge storage, giving rise to ultrahigh values of

20 4700 F g^{-1} for specific capacitance of the electrode and 163 Wh kg^{-1} for average energy

capacity. These results particularly need to be considered since the charging energy had been

underestimated and discharging energy been overestimated in comparison with the symmetric

triangular GCD plot of an ideal capacitor (the red dashed plot in **Fig.** 15). This is because the

calculated energy is the area under the dashed straight lines, whereas, the actual energy is the

area under the curved solid lines. The charging energy is larger than the discharging one,

reflecting the electrode reaction being not fully reversible and hence only a portion of the
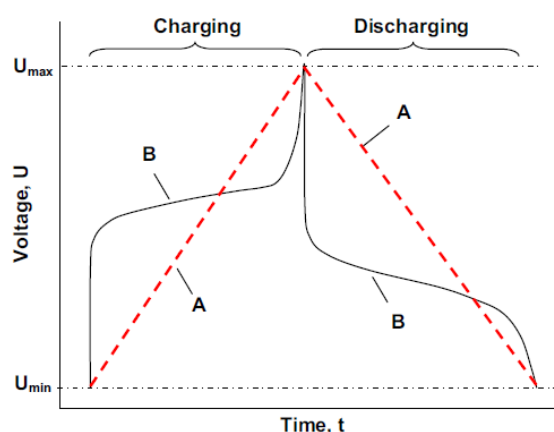
Fig. 15. Schematic comparison of the GCD plot of a quasi-reversible faradaic reaction such

as the case in **Fig.** 14 (black solid lines) with that of an ideal capacitive faradaic reaction (red

dashed lines). The area under the potential curve of the GCD is proportional to the energy

consumed (or released) during charging (or discharging) [43].

energy used during the charging period was released during the discharging period. In this

case, the energy efficiency considered as the ratio of discharging energy to charging energy is

far smaller than 1, which is not ideal for energy storage.

Different charge storage mechanisms have been briefly introduced, including non-

faradaic EDL storage or capacitive faradaic pseudocapacitance and non-capacitive faradaic

battery-like behaviours. However, classification of individual charge storage mechanisms has

become rather ambiguous since the emergence of advanced composite electrode materials

(e.g. the composites of carbon materials with ECPs [16] or transition metal oxides [44]) or

the application of a novel redox active electrolyte [42]). Confusions therefore appeared in the literature [39, 45-47] in terms of understanding of the origin of pseudocapacitance and determination of capacitance. Although Conway had stated an average pseudocapacitance of a battery could be determined by dividing the withdrawable charge (ΔQ) with the voltage difference (ΔE) in 1991, he simultaneously emphasised that the discharge characteristics of Q vs. time would not be similar as those of a capacitor, which is not very useful and informative and could be misleading [48]. Hence, it is essential and crucial to carefully define and differentiate the charge storage process according to the electrochemistry of the electrode materials and from the viewpoint of the semiconductor or delocalisation band theory. This is certainly significant and helpful to precisely evaluate the performance of supercapacitors and beneficial for designing practical devices for energy storage, such as supercapattery.

4. Energy capacity enhanced by unequal capacitance

4.1. Unequal capacitance theory

It is well known that supercapacitors are high power energy storage devices, but relatively low in energy capacity compared to batteries. There is a strong desire for improving the energy capacity of supercapacitors. In theory, this improvement can be achieved by either increasing the capacitance or expending the working voltage of a supercapacitor based on Eq. (5), where ε represents the energy stored in a supercapacitor, C capacitance and U voltage.

For symmetrical supercapacitors, capacitance equalisation of the two electrodes is necessary to maximise material utilisation and specific energy storage capacity, because the positive and negative electrodes have the same working potential range. Practically, one should also consider if the open circuit potential (OCP) of the material is at the centre of the potential range [49], because the OCP does not always match the potential of zero charge

(PZC) with reference to **Fig.** 16. However, it may not be the same case in asymmetrical

supercapacitors. The amount of charge, Q, stored in the positive and negative electrodes in an

asymmetrical supercapacitor must be the same and is governed by Eq. (12) to (14),

$$Q = C_P U_P = C_N U_N \text{ or } U_N = U_P C_P / C_N \tag{12}$$

$$C = \frac{C_P C_N}{C_P + C_N} = \frac{C_P}{1 + C_P/C_N} \tag{13}$$

$$U = U_P + U_N = U_P\left(1 + C_P/C_N\right) \tag{14}$$

where C_P and C_N are the capacitance, and U_P and U_N are the "working potential range" of the

positive and negative electrodes in the cell. Note that U_P or U_N is defined as the difference

between the more positive (or less negative) and less positive (or more negative) potential

limits of the working potential range. It means that U_P or U_N is always positive, disregarding

the electrode's polarity.

Another upper and lower limit, "exploitable potential range" for positive or negative

electrode, U^o_P or U^o_N, is set by any irreversible electrode reactions in a supercapacitor cell,

such as solvent decomposition and over-oxidation or over-reduction of the electrode

materials. Thus, $U_P \leq U^o_P$ and $U_N \leq U^o_N$. Eq. (15) describes the relationship among U, U_P, U_N,

U^o_P and U^o_N. (Note: $U^o_P = \text{CPR}(+)$ and $U^o_N = \text{CPR}(-)$ in **Fig.** 16.)

$$U = U_N + U_P \leq U^o_P + U^o_N \tag{15}$$

Along the potential axis, U_P and U_N are next to each other, but U^o_P and U^o_N could be either

connected or overlapping partially or completely. From Eq. (12), it can be found that if C_P

increases, U_P will reduce and the same correlation applies to C_N and U_N. For a symmetrical

supercapacitor, the above situation is avoided because of the equalised electrode capacitance

(*i.e.* $C_N = C_P$). In the case of an asymmetrical supercapacitor, the two electrodes have likely

different values for U^o_P and U^o_N. When the positive and negative electrodes are equalised in

capacitance, the cell voltage will be limited either by the positive electrode if $U^o_P < U^o_N$, or

by the negative electrode if $U^o_P > U^o_N$. In cases where U^o_P and U^o_N overlap, they should be replaced by U_P and U_N respectively. However, the voltage of an asymmetrical supercapacitor can also be extended by increasing the capacitance of the "cell voltage limiting electrode", leading to the increase of the energy stored by the supercapacitor as indicated in Eq. (16) which is derived from Eq. (5) and (12) to (14).

$$E = \frac{1}{2}CU^2 = \frac{1}{2}C_PU_P^2(1 + C_P/C_N) \tag{16}$$
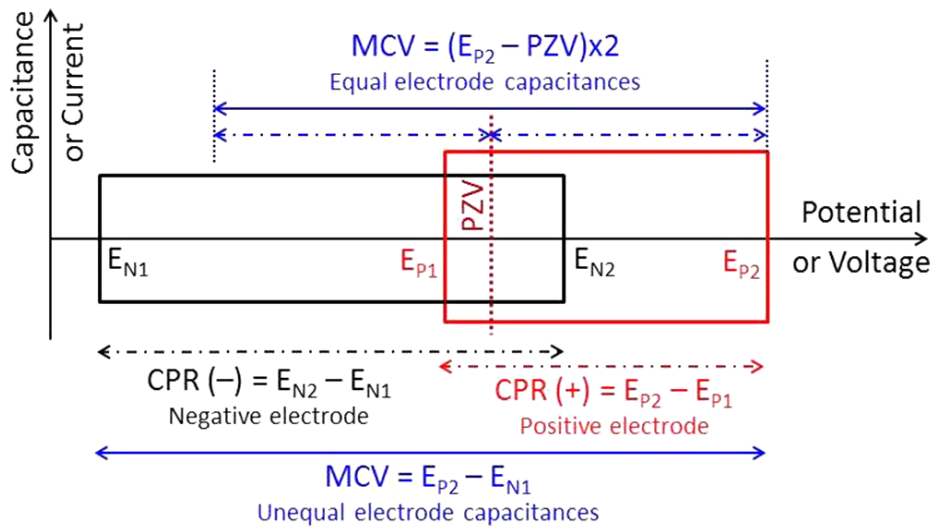
Fig. 16. A model of supercapacitor voltage. Schematic illustration of supercapacitor maximum charging voltage (MCV), potential of zero voltage (PZV) and electrode capacitive potential range (CPR) [50]. CPR(+) = U^o_P and CPR(−) = U^o_N in Eq. (15).

It has been proven that the positive to negative electrode capacitance ratio (C_P/C_N) plays an important role in the improvement of a practical asymmetrical supercapacitors without changing the materials [51]. Along with C_P/C_N, the capacitive potential range (CPR) and potential of zero voltage (PZV) may affect the maximum charging voltage (MCV) and stored energy of the supercapacitor. **Fig.** 16 shows a model of supercapacitor voltage [50]. The lower and upper potential limits of the negative and positive electrodes are denoted as E_{N1},

1   E_{N2}, E_{P1} and E_{P2}, respectively. The CPR of the negative or positive electrode is $E_{N2} - E_{N1}$ or

2   $E_{P2} - E_{P1}$, respectively. PZV is defined as the equal electrode potential when a supercapacitor

3   is fully discharged and its voltage is zero if $E_{N2} \geq E_{P1}$. PZV affects the coulombic efficiency

4   and the MCV of a supercapacitor, but is difficult to predict in practice. As shown in **Fig.** 16,

5   if the positive electrode is the "cell voltage limiting electrode" as the MCV of the

6   supercapacitor is determined by E_{P2}, then $PZV - E_{N1} > E_{P2} - PZV$, and the capacitance of the

7   two electrodes are equal, the MCV would be $(E_{P2} - P_{ZV}) \times 2$.

8

9   4.2. Asymmetrical supercapacitor

10   A few asymmetrical supercapacitor examples have proved the practicality of the

11 unequal capacitance theory [50, 51]. An asymmetrical supercapacitor composing of a PAN-

12 CNT nanocomposites positive electrode and a CMPB (Cabot Monarch 1300pigment black)

13 negative electrode has been investigated [51]. PAN has very high theoretical specific

14 capacitance (750 F g^{-1}) [40] and excellent charging-discharging cycle stability [16], but it has

15 a small exploitable potential range of 0.7 - 0.8 V in acidic aqueous electrolytes [16]. If PAN

16 is used in a symmetrical supercapacitor, its energy capacity and power capability are

17 compromised, as indicated in Eq. (5), despite of the polymer's ultrahigh specific capacitance.

18 In the previous research [51], several PAN-CNT positive electrodes were prepared at

19 deposition charges of 166 to 312 mC, corresponding to C_P/C_N ratios of 0.8 to 1.5. **Fig.** 17

20 shows the CVs of these PAN-CNT (+)|HCl (1.0 M)|CMPB (−) asymmetrical supercapacitors.

21 In this supercapacitor, the positive electrode PAN-CNT (+) is the "cell voltage limiting

22 electrode" [51]. In **Fig.** 17, the charging peaks can be identified on all these CVs near the

23 high voltage ends and the peak voltage shifted to higher values with increasing C_P/C_N ratio.

24 When the C_P/C_N ratio changes from 1.0 to 1.5, the cell capacitance only decreases by 7%,

25 while the specific energy of the cell increases over 80%. These improvements are remarkable,

as there was only a small increase of 12.9% in the total mass of the electrode materials.
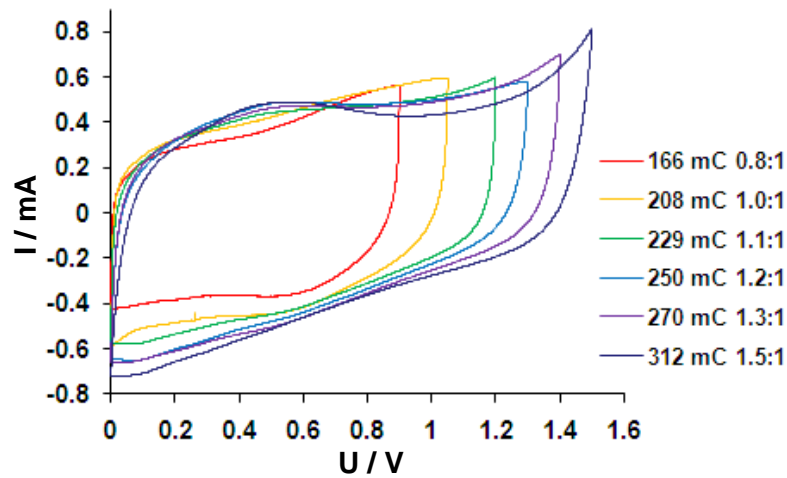
Fig. 17. CVs of asymmetrical supercapacitors with a 0.3 mg CMPB negative electrode and a PAN-CNT positive electrode at indicated C_P/C_N ratios without the charging current peek. Scan rate: 20 mV s^{-1} [51].

Similar asymmetrical supercapacitor composing of polypyrrole-CNT (PPy-CNT) composites positive electrode and CMPB negative electrode have been fabricated and tested. The relative research is still ongoing and unpublished. The preliminary data indicates that the asymmetrical cell can improve the cell voltage form 1.0 to 1.4 V and cell specific energy from 13.0 to 16.6 J g^{-1} comparing to the symmetrical cell. Recently, graphenes are popularly used to form composite with conducting polymers that could increase supercapacitor cell voltage when combined with suitable counter electrode and electrolyte [52].

4.3. Unit cell supercapacitor

Conventionally, a symmetrical aqueous carbon-carbon supercapacitor is perceived to show a narrower working voltage than an asymmetrical supercapacitor. However, recent study suggested that a unit cell supercapacitor consisting of CMPB can reach beyond 1.9 V in

1 cell voltage, and retain over 85% of the initial capacitance through 10,000 cycles with the cell

2 becoming stable after the $1,000^{th}$ cycles [53]. **Fig.** 18 shows the CVs of CMPB in 0.3 M

3 K_2SO_4 solution at a scan rate of 5 mV s^{-1} [53]. Basically, the negative current reflects the rate

4 of absorption/adsorption of hydrated cations, H_3O^+ and K^+, and desorption of anion, SO_4^{2-},

5 during the negative polarisation. The positive current corresponds to the rate of desorption of

6 the mentioned cations and absorption/adsorption anions in the course of positive polarisation.

7 It is also noticed that there is small positive current humps between 0.4 and 0.5 V on the CVs

8 when the negative potential limit reached beyond -1.0 V, where a fast increasing negative

9 current appeared due to the formation of hydrogen on the electrode. Actually, the current

10 humps locate in a very positive potential range. It suggests that the hydrogen is trapped in the

11 in the nanopores of CMPB at high negative polarisation.

12 The SEM and TEM images of the CMPB used in the research are shown in **Fig.** 19 and

13 reveal micrometer sized aggregates of uniform onion-like spherical nanoparticles (10 nm)

14 [54]. This nanoporous structure could also make contribution to the extension of the negative

15 potential limit away from the theoretical value of water decomposition [55].
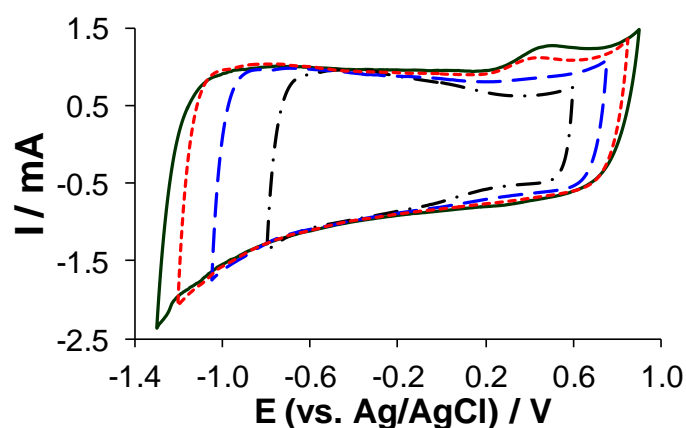
16

17 **Fig. 18.** CVs of the conventional three-electrode cell using the CMPB-PTFE (2.5 mg) coated

18 graphite disc working electrode in 0.3 M K_2SO_4 solution over different working potential

19 windows. Scan rate: 5 mV s^{-1} [53].
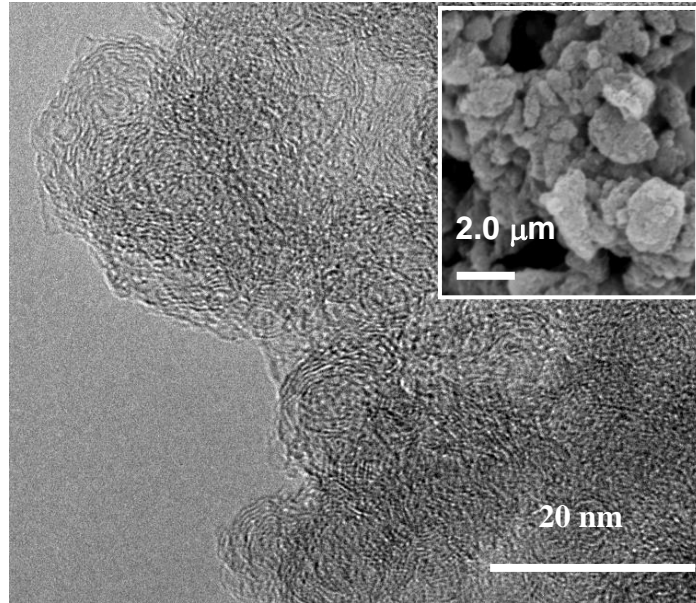
Fig. 19. TEM and SEM (insert) images of the CMPB [54].

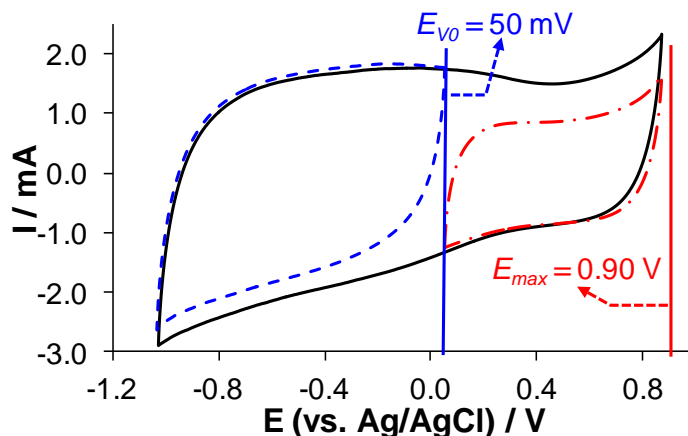**Fig.** 20 shows the CVs of CMPB-PTFE (1.0 mg) in the conventional three-electrode cell with the PZV of 50 mV and potential ranges with unequal electrode capacitance [53]. The C_P/C_N ratio comes to 4/3 and has successfully extended the negative electrode potential windows towards a more negative range. Meanwhile, the positive electrode potential windows kept the same, but the cell voltage increased from 1.6 V ($C_P/C_N = 1$) to 1.9 V ($C_P/C_N = 4/3$). The energy capacity and capacitance have been compared between equal and unequal electrode capacitance CMPB supercapacitors. **Fig.** 21 shows the capacitance retention of supercapacitor with different C_P/C_N ratios [53]. It can be found that the supercapacitor with the $C_P/C_N$ ratio of 4/3 performs better than the one with the ratio of 1. The calculation of the cell capacitance and specific energy capacity indicate that there will be only 2% decrease of the cell capacitance but 38% increase of the cell specific energy capacity. This is a typical zero cost engineering example.

Fig. 20. CVs of CMPB-PTFE (1.0 mg) in the conventional three-electrode cell with the PZV of 50 mV and potential ranges with unequal electrode capacitance [53].
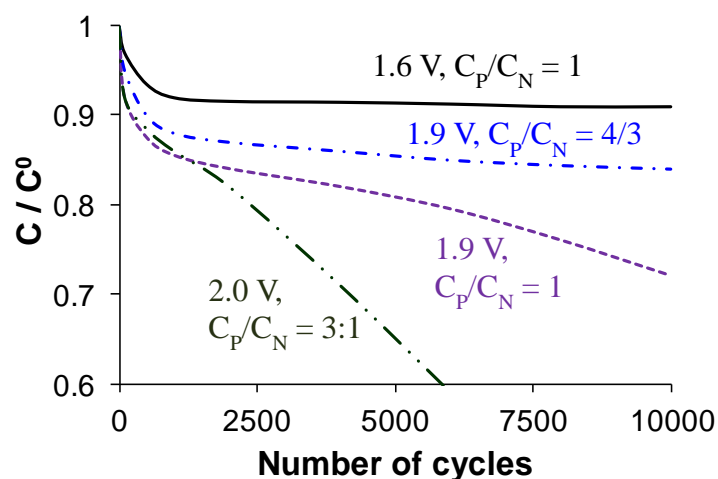
Fig. 21. Capacitance retention (C/C^0) as a function of the number of charge-discharge cycles of sandwich-type supercapacitors with the cell voltage limit indicated [49].
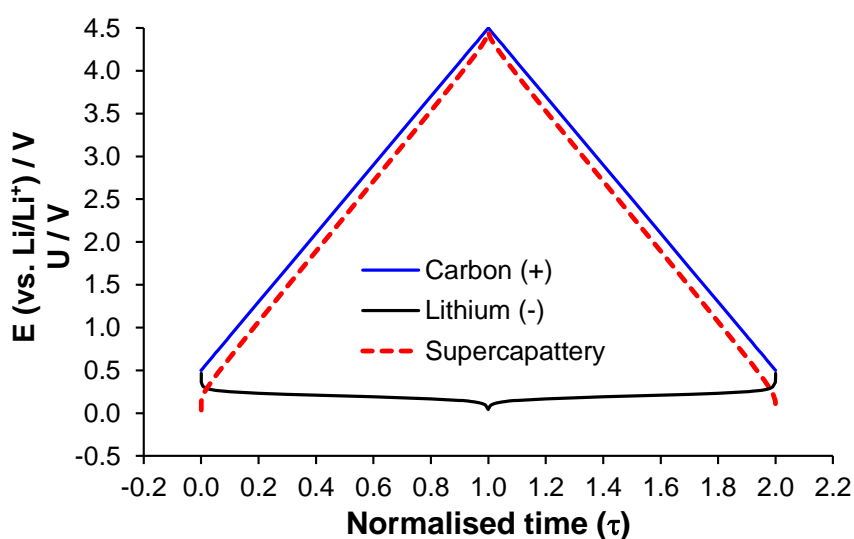
5. Supercapattery

Another widely applied approach to increasing the energy capacity of supercapacitors is using hybrid configurations that take the advantages of both the supercapacitor and battery. The particular design involves combination of a supercapacitor electrode with a battery electrode, such as the so called lithium ion capacitor [56] and the more general term supercapattery (= **supercapa**citor + ba**ttery**) [50, 57].

Theoretically, the hypothetical battery of lithium metal and fluorine gas (Li-F battery)

would output a cell voltage about 6.1 V and offer a specific energy content of 6304 Wh/kg at room temperature. This value sets the upper limit of specific energy for all batteries. For Li-ion batteries (e.g. Li_xC_6 | $Li_{1-x}CoO_2$), the theoretical specific energy is 552 Wh/kg at 3.5 V. If one considers a supercapattery with a lithium metal negative electrode and a supercapacitor positive electrode of 400 F/g, the specific energy value would be 625 Wh/kg for the cell voltage to vary from 3.5 V to 1.0 V. In this calculation, the mass of the lithium metal is negligible because the specific charge capacity of lithium is much larger than that of the supercapacitor electrode. Thus, in theory, supercapattery can possess higher specific energy than both battery and supercapacitor, and should be able to supply this specific energy at a power output almost as high as supercapacitor with suitable electrode and cell designs.

Nanostructured carbons, such as activated carbon, CNT and graphene represent the primary material choices for the polarisable capacitor-like electrode (i.e. capacitive non-faradaic) owing to their large surface area, porosity, stability over a wide potential window, as well as intrinsically low electrical resistance. Pseudo-capacitive materials including MnO_2, RuO_2 and conducting polymers can also be used to gain higher electrode capacitance which however also means narrower potential windows. As to the battery-like electrode, a much wider choice of materials exists, from lead acid battery to metal/air systems, but metal compounds such as SnO_2, MnO_2 and $LiFePO_4$ are more practically and commercially available. It should be mentioned that combining the supercapacitor and battery electrodes into one device could result in performance very close to that of the supercapacitor [1, 50]. This is demonstrated by the calculated GCD plots shown in **Fig.** 22 for a cell with a lithium metal negative electrode and an activated carbon positive electrode. In the calculation, the potential range of the activated carbon is set between 0.5 V and 4.5 V vs. Li/Li^+ to avoid interaction of the carbon with lithium metal. With overall cell performance being comparable to that of a supercapacitor, the analysis and comparison can follow those capacitor equations.

1　　Examples of such capacitive cell behaviour are also reported in the literature [58, 59]. On the

2　　other hand, the combination of battery and supercapacitor electrodes may also present battery

3　　like features as that shown in **Figs.** 14 and 15. In such cases, data presentation and analysis

4　　should follow those for batteries. Particularly, specific charge capacity (e.g. mAh g^{-1}) should

5　　be reported, instead of specific capacitance (F g^{-1}). For hybrid devices showing rechargeable

6　　battery behaviour, the term supercabattery is recommended [50].

8　　**Fig. 22.** Calculated potentials of the positive activated carbon electrode (blue solid line) and

9　　the lithium metal negative electrode (solid black line) and the cell voltage (dashed red line)

10　　for a "Li | activated carbon" supercapattery.

11

12　　Recent studies reveal that an aqueous supercapattery consisting of a MnO_2 positive

13　　electrode and a Li/LISICON/PEO-LiTFSI/Li$^+$ negative electrode had achieved a specific

14　　energy value of 114 Wh kg^{-1} with a 4.3 V cell voltage [60]. The specific energy can come to

15　　520 Wh kg^{-1} with a 3.8 V cell voltage, if the positive electrode is replaced by RuO_2 [60].

16　　However, the current density of the supercapattery discussed above is 0.255 mA cm^{-2}, which

17　　is still not ideal for high power application. Our recent supercapattery work based on an

18　　activated carbon (110 F g^{-1}) positive electrode and a Li/Li$^+$ negative electrode using an ionic

1   liquid electrolyte can achieve a specific energy value of 200 Wh kg^{-1} at a 1.0 mA cm^{-2} current

2   density. The relative work is still ongoing and will be published elsewhere [61].

3

4   6. Conclusions

5   In this paper, we have proposed to define and differentiate **capacitive** and **non-**

6   **capacitive** faradaic processes for charge storage in supercapacitors according to the band

7   theory which the origin of pseudocapacitance has been correlated with electron transfer to or

8   from the conduction band of semiconductor type materials. The principle and performance

9   governing equations of conventional capacitors have been presented and applied to

10   differentiate between batteries and supercapacitors based on the shapes of CVs and GCDs. It

11   is confirmed that pseudocapacitance is featured by rectangular CVs and triangular GCDs and

12   peak-shaped CVs and non-linear GCDs are features of battery behaviour which should not be

13   used for measurement of capacitance values and energy estimation.

14   We have also found a unique affinity between Ca^{2+} ions and the oxy-groups on the

15   surfaces of CNTs, leading to a significant capacitance improvement. The specific capacitance

16   of the CNTs measured in CaCl$_2$ based electrolytes was generally higher than that in more

17   commonly used alkali salts based electrolytes. This understanding is new to supercapacitor

18   research and could have a significant impact on development of supercapacitors based on

19   CNTs, graphenes and/or activated carbons which are all enriched with various surface oxy-

20   groups. In particular, after mixing with FA and H$_2$O, the resultant organoaqueous CaCl$_2$

21   electrolyte enabled the CNTs to store charges at both room and sub-zero temperatures below

22   −60 $^{\circ}$C without a significant capacitance loss.

23   On the other hand, energy capacity enhancement by unequal capacitances has been

24   demonstrated in theory and examples. It clear shows that the phenomena of the potential of

25   zero voltage (PZV), capacitive potential range (CPR) and positive to negative electrode

capacitance ratio (C_P/C_N) affect the performance of supercapacitors. It also shows that for energy enhancement, the capacitance unequalisation approach could be very low or almost zero in engineering cost. The recent development in supercapattery that utilises both capacitive and non-capacitive charge storage mechanisms (i.e. hybrid devices combining supercapacitor and battery electrodes) reveals much increased energy capacity comparable or higher than those existing rechargeable batteries, including the lithium ion battery. These initial studies have demonstrated a very promising prospect of supercapattery.

Reference

[1] A.J. Stevenson, D.G. Gromadskyi, D. Hu, J.H. Chae, L. Guan, L.P. Yu, G.Z. Chen, Supercapatteries with hybrids of redox active polymers and nanostructured carbons, in: X.L. Feng (Ed.) Nanocarbons for advanced energy storage, Wiley-VCH, Weinheim, 2015, 179-210.

[2] F. Chen, Q. Sun, W. Gao, J. Liu, C. Yan, Q. Liu, Study on a high current density redox flow battery with Tin(II)/Tin as negative couple, Journal of Power Sources, 280 (2015) 227-230.

[3] J.H. Chae, K.C. Ng, G.Z. Chen, Nanostructured materials for the construction of asymmetrical supercapacitors, Proceedings of the Institution of Mechanical Engineers Part a-Journal of Power and Energy, 224 (2010) 479-503.

[4] G.Z. Chen, Understanding supercapacitors based on nano-hybrid materials with interfacial conjugation, Progress in Natural Science-Materials International, 23 (2013) 245-255.

[5] H. Zhang, G. Cao, Y. Yang, Carbon nanotube arrays and their composites for electrochemical capacitors and lithium-ion batteries, Energy & Environmental Science, 2 (2009) 932-943.

[6] H. Pan, J. Li, Y.P. Feng, Carbon nanotubes for supercapacitor, Nanoscale Research Letters, 5 (2010) 654-668.

[7] T.S. Hyun, H.L. Tuller, D.Y. Youn, H.G. Kim, I.D. Kim, Facile synthesis and electrochemical properties of RuO_2 nanofibers with ionically conducting hydrous layer, Journal of Materials Chemistry, 20 (2010) 9172-9179.

[8] L. Dai, D.W. Chang, J.B. Baek, W. Lu, Carbon nanomaterials for advanced energy conversion and storage, Small, 8 (2012) 1130-1166.

[9] J.H. Chae, X.H. Zhou, G.Z. Chen, From electrochemical capacitors to supercapatteries, Green, 2 (2012) 41-54.

[10] C.G. Liu, M. Liu, F. Li, H.M. Cheng, Frequency response characteristic of single-walled carbon nanotubes as supercapacitor electrode material, Applied Physics Letters, 92 (2008).

[11] F. Zhao, A. Vicenzo, M. Hashempour, M. Bestetti, Supercapacitor electrodes by direct growth of multi-walled carbon nanotubes on Al: A study of performance versus layer growth evolution, Electrochimica Acta, 150 (2014) 35-45.

[12] S. Hussain, R. Amade, H. Moreno, E. Bertran, RF-PECVD growth and nitrogen plasma functionalization of cnts on copper foil for electrochemical applications, Diamond and Related Materials, 49 (2014) 55-61.

[13] D. Zilli, P.R. Bonelli, A.L. Cukierman, Effect of alignment on adsorption characteristics of self-oriented multi-walled carbon nanotube arrays, Nanotechnology, 17 (2006) 5136-5141.

[14] C.M. Niu, E.K. Sichel, R. Hoch, D. Moy, H. Tennent, High power electrochemical capacitors based on carbon nanotube electrodes, Applied Physics Letter, 70 (1997) 1480-1482.

[15] K.H. An, W.S. Kim, Y.S. Park, J.M. Moon, D.J. Bae, S.C. Lim, Y.S. Lee, Y.H. Lee, Electrochemical properties of high-power supercapacitors using single-walled carbon nanotube electrodes, Advanced Functional Materials, 11 (2001) 387-392.

[16] C. Peng, Jin, J., G.Z. Chen, A comparative study on electrochemical co-deposition and capacitance of composite films of conducting polymers and carbon nanotubes, Electrochimica Acta, 53 (2007) 525-537.

[17] X.L. Chen, W.S. Li, C.L. Tan, W. Li, Y.Z. Wu, Improvement in electrochemical capacitance of carbon materials by nitric acid treatment, Journal of Power Sources, 184 (2008) 668-674.

[18] C.C. Hu, C.C. Wang, Effects of electrolytes and electrochemical pretreatments on the capacitive characteristics of activated carbon fabrics for supercapacitors, Journal of Power Sources, 125 (2004) 299-308.

[19] F.C. Wu, R.L. Tseng, C.C. Hu, C.C. Wang, Physical and electrochemical characterization of activated carbons prepared from firwoods for supercapacitors, Journal of Power Sources, 138 (2004) 351-359.

[20] F.C. Wu, R.L. Tseng, C.C. Hu, C.C. Wang, The capacitive characteristics of activated carbons—comparisons of the activation methods on the pore structure and effects of the pore structure and electrolyte on the capacitive performance, Journal of Power Sources, 159 (2006) 1532-1542.

[21] Y. Tian, J.W. Yan, R. Xue, B.L. Yi, Influence of electrolyte concentration and temperature on the capacitance of activated carbon, Acta Physico-Chimica Sinica, 27 (2011) 479-485.

[22] J.H. Chae, G.Z. Chen, Influences of ions and temperature on performance of carbon nano-particulates in supercapacitors with neutral aqueous electrolytes, Particuology, 15 (2014) 9-17.

[23] K. Esumi, M. Ishigami, A. Nakajima, K. Sawada, H. Honda, Chemical treatment of carbon nanotubes, Carbon, 34 (1996) 279-281.

[24] H.A. Andreas, B.E. Conway, Examination of the double-layer capacitance of an high specific-area C-cloth electrode as titrated from acidic to alkaline phs, Electrochimica Acta, 51 (2006) 6510-6520.

[25] Y. Gao, Z. Qin, L. Guan, X. Wang, G.Z. Chen, Organoaqueous calcium chloride electrolytes for capacitive charge storage in carbon nanotubes at sub-zero-temperatures, Chemical Communications, 51 (2015) 10819-10822.

[26] K. Yang, Z.L. Yi, Q.F. Jing, D.H. Lin, Dispersion and aggregation of single-walled carbon nanotubes in aqueous solutions of anionic surfactants, Journal of Zhejiang University-Science A, 15 (2014) 624-633.

[27] H. Wang, H. Nie, Y. Wang, Y. Chang, E. Dong, S. Yang, Purifying carbon nanotube polluted water involves adding calcium chloride aqueous solution with carbon nanotube aqueous solution, mixing mixture and storing it to sediment particles, and obtaining colorless transparent water, Univ Shanghai.

[28] R. Garcia-Fandino, M.S.P. Sansom, Designing biomimetic pores based on carbon nanotubes, Proceedings of the National Academy of Sciences of the United States of America, 109 (2012) 6939-6944.

[29] L.P. Zanello, B. Zhao, H. Hu, R.C. Haddon, Bone cell proliferation on carbon nanotubes, Nano Letters, 6 (2006) 562-567.

[30] E. Perricone, M. Chamas, L. Cointeaux, J.C. Lepretre, P. Judeinstein, P. Azais, F. Beguin, F. Alloin, Investigation of methoxypropionitrile as co-solvent for ethylene carbonate

based electrolyte in supercapacitors. A safe and wide temperature range electrolyte,

Electrochimica Acta, 93 (2013) 1-7.

[31] W.Y. Tsai, R. Lin, S. Murali, L.L. Zhang, J.K. Mcdonough, R.S. Ruoff, P.L. Taberna, Y.

Gogotsi, P. Simon, Outstanding performance of activated graphene based supercapacitors in

ionic liquid electrolyte from -50 to 80 degrees C, Nano Energy, 2 (2013) 403-411.

[32] E.J. Brandon, W.C. West, M.C. Smart, L.D. Whitcanack, G.A. Plett, Extending the low

temperature operational limit of double-layer capacitors, Journal of Power Sources, 170

(2007) 225-232.

[33] http://www.fhwa.dot.gov/publications/research/safety/95202/95005.cfm.

[34] S.W. Zhang, G.Z. Chen, Manganese oxide based materials for supercapacitors, Energy

Materials, 3 (2008) 186-200.

[35] A.J. Bard, L.R. Faulkner, Electrochemical methods: Fundamentals and applications,

John Wiley &Sons, New York, 2001.

[36] C. Peng, X.H. Zhou, G.Z. Chen, F. Moggia, F. Fages, H. Brisset, J. Roncali, Internally

referenced analysis of charge transfer reactions in a new ferrocenyl bithiophenic conducting

polymer through cyclic voltammetry, Chemical Communications, (2008) 6606-6608.

[37] M.Q. Wu, G.A. Snook, G.Z. Chen, D.J. Fray, Redox deposition of manganese oxide on

graphite for supercapacitors, Electrochemistry Communications, 6 (2004) 499-504.

[38] C. Peng, D. Hu, G.Z. Chen, Theoretical specific capacitance based on charge storage

mechanisms of conducting polymers: Comment on 'vertically oriented arrays of polyaniline

nanorods and their super electrochemical properties', Chemical Communications, 47 (2011)

4105-4107.

[39] B.K. Kuila, B. Nandan, M. Boehme, A. Janke, M. Stamm, Vertically oriented arrays of

polyaniline nanorods and their super electrochemical properties, Chemical Communications,

(2009) 5749-5751.

[40] K. Lota, V. Khomenko, E. Frackowiak, Capacitance properties of poly(3,4-ethylenedioxythiophene)/carbon nanotubes composites, Journal of Physics and Chemistry of Solids, 65 (2004) 295-301.

[41] W.J. Albery, Z. Chen, B.R. Horrocks, A.R. Mount, P.J. Wilson, D. Bloor, A.T. Monkman, C.M. Elliott, Spectroscopic and electrochemical studies of charge-transfer in modified electrodes, Faraday Discussions, 88 (1989) 247-259.

[42] L.Q. Mai, A. Minhas-Khan, X.C. Tian, K.M. Hercule, Y.L. Zhao, X. Lin, X. Xu, Synergistic interaction between redox-active electrolyte and binder-free functionalized carbon for ultrahigh supercapacitor performance, Nature Communications, 4 (2013) 2923.

[43] B. Akinwolemiwa, C. Peng, G.Z. Chen, Redox electrolytes in supercapacitors, Journal of the Electrochemical Society, 162 (2015) A5054-A5059.

[44] X.B. Jin, W.Z. Zhou, S.W. Zhang, G.Z. Chen, Nanoscale microelectrochemical cells on carbon nanotubes, Small, 3 (2007) 1513-1517.

[45] H. Wang, H.S. Casalongue, Y. Liang, H. Dai, Ni(OH)(2) nanoplates grown on graphene as advanced electrochemical pseudocapacitor materials, Journal of the American Chemical Society, 132 (2010) 7472-7477.

[46] P.A. Mini, A. Balakrishnan, S.V. Nair, K.R.V. Subramanian, Highly super capacitive electrodes made of graphene/poly(pyrrole), Chemical Communications, 47 (2011) 5753-5755.

[47] D.D. Zhao, M.W. Xu, W.H. Zhou, J. Zhang, H.L. Li, Preparation of ordered mesoporous nickel oxide film electrodes via lyotropic liquid crystal templated electrodeposition route, Electrochimica Acta, 53 (2008) 2699-2705.

[48] B.E. Conway, Transition from supercapacitor to battery behavior in electrochemical energy-storage, Journal of the Electrochemical Society, 138 (1991) 1539-1548.

[49] T.H. Wu, C.T. Hsu, C.C. Hu, L.J. Hardwick, Important parameters affecting the cell voltage of aqueous electrical double-layer capacitors, Journal of Power Sources, 242 (2013)

289-298.

[50] Z. Dai, C. Peng, J.H. Chae, K.C. Ng, G.Z. Chen, Cell voltage versus electrode potential range in aqueous supercapacitors, Scientific Reports, 5 (2015).

[51] C. Peng, S.W. Zhang, X.H. Zhou, G.Z. Chen, Unequalisation of electrode capacitances for enhanced energy capacity in asymmetrical supercapacitors, Energy & Environmental Science, 3 (2010) 1499-1502.

[52] Y.J. Peng, T.H. Wu, C.T. Hsu, S.M. Li, M.G. Chen, C.C. Hu, Electrochemical characteristics of the reduced graphene oxide/carbon nanotube/polypyrrole composites for aqueous asymmetric supercapacitors, Journal of Power Sources, 272 (2014) 970-978.

[53] J.H. Chae, G.Z. Chen, 1.9 V aqueous carbon-carbon supercapacitors with unequal electrode capacitances, Electrochim. Acta, 86 (2012) 248-254.

[54] X. Zhou, C. Peng, G.Z. Chen, 20 V stack of aqueous supercapacitors with carbon (-), titanium bipolar plates and CNT-polypyrrole composite (+), AIChE J., 58 (2012) 974-983.

[55] K. Jurewicz, E. Frackowiak, F. Béguin, Towards the mechanism of electrochemical hydrogen storage in nanostructured carbon materials, Applied Physics A, 78 (2004) 981-987.

[56] S.W. Woo, K. Dokko, H. Nakano, K. Kanamura, Bimodal porous carbon as a negative electrode material for lithium-ion capacitors, Electrochemistry, 75 (2007) 635-640.

[57] D. Hu, C. Peng, G.Z. Chen, Electrodeposition of nonconducting polymers: Roles of carbon nanotubes in the process and products, ACS Nano, 4 (2010) 4274-4282.

[58] C.T. Hsu, C.C. Hu, Synthesis and characterization of mesoporous spinel $NiCo_2O_4$ using surfactant-assembled dispersion for asymmetric supercapacitors, Journal of Power Sources, 242 (2013) 662-671.

[59] J.C. Chen, C.T. Hsu, C.C. Hu, Superior capacitive performances of binary nickel-cobalt hydroxide nanonetwork prepared by cathodic deposition, Journal of Power Sources, 253 (2014) 205-213.

[60] S. Makino, Y. Shinohara, T. Ban, W. Shimizu, K. Takahashi, N. Imanishi, W. Sugimoto, 4 V class aqueous hybrid electrochemical capacitor with battery-like capacity, RSC Adv., 2 (2012) 12144-12147.

[61] L.P. Yu, G.Z. Chen, High energy supercapattery with an ionic liquid solution of LiClO4, Faraday Discuss. (2006) DOI: 10.1039/C5FD00232J